Reflectance spectra (1-5 μm) at low temperatures and different grain sizes of ammonium-bearing minerals relevant for icy bodies

M. Fastelli, P. Comodi, B. Schmitt, P. Beck, O. Poch, P. Sassi, A. Zucchini

This is the Accepted Manuscript of this published paper: M. Fastelli, P. Comodi, B. Schmitt, P. Beck, O. Poch, P. Sassi, A. Zucchini, Reflectance spectra (1–5 µm) at low temperatures and different grain sizes of ammonium-bearing minerals relevant for icy bodies, Icarus 382, 115055, 2022. https://doi.org/10.1016/j.icarus.2022.115055

Reflectance spectra (1-5 µm) at low temperatures and different grain sizes of ammonium-bearing minerals relevant for icy bodies.

M. Fastelli[a*], P. Comodi[a]; B. Schmitt[b], P. Beck[b], O. Poch[b], P. Sassi[c], A. Zucchini[a]

a Department of Physics and Geology, University of Perugia, I-06123, Perugia, Italy

b Univ. Grenoble Alpes, CNRS, IPAG, 38000 Grenoble, France

c Department of Chemistry, Biology and Biotechnology, University of Perugia, Via Elce di sotto 8, 06123 Perugia, Italy

Keywords: Ammonium-bearing minerals, reflectance, low temperature, mineralogy, icy bodies

*Email: maximiliano.fastelli@studenti.unipg.it – maximiliano.fastelli@gmail.com

Phone: +39 3495410743

Address: Department of Physics and Geology, University of Perugia, I-06123, Perugia, Italy

Highlights:

- Reflectance spectra (1-5 µm) of ammonium minerals at low temperatures.
- NH_4^+ overtone and combination bands characterize sample spectra.
- Phase transitions, when they occur, affect the band parameters, especially the position.

Abstract

It has been proposed that ammonium-bearing minerals are present in a varying amount in icy planetary bodies. Their observation at the surface of large objects was related to the upwelling and cryovolcanism of ammoniated water from possible subsurface oceans forming ammonium-bearing minerals (NH_4^+) mixed with ice at the surface. We analyzed the temperature evolution of the near-infrared spectra of a selected number of anhydrous and hydrated ammonium-bearing minerals containing different anions and water content. Reflectance spectra were collected in the 1-4.8 µm spectral range at cryogenic temperatures ranging from 293K to ~65K and the effect of sample's grain size between 32 and 150 µm was also investigated at room temperature. Reflectance spectra of anhydrous samples show well-defined absorption bands in the 1-2.5 µm range. The bands located at ~ 1.06, 1.3, 1.56, 2.02, and 2.2 µm could be useful to discriminate these salts and their characteristics are examined in detail in this work. On the other hand, the reflectance spectra of water-rich samples show H_2O fundamental absorption bands strongly overlapping the NH_4^+ bands, thus dominating the spectra from 1 to 2.8 µm and fully saturating above 2.8 µm. The position of the absorption bands changes with temperature and grain size, shifting to higher frequencies as temperature decreases. The low-temperature spectra also reveal a fine structure compared to the room temperature ones and display narrower and more defined absorption bands. Granulometry mainly affects the band depth and band area parameters. Moreover, mascagnite, salammoniac, ammonium phosphate, tschermigite, and ammonium nitrate are subjected to a reversible low-temperature phase transition, which is

manifested in the spectra by a progressive growth and shift of the bands toward shorter wavelengths with an abrupt change in their depth. This new set of spectra at cryogenic temperatures can be directly compared with remote sensing data to detect the presence of ammonium-bearing minerals on the surface of icy bodies. Their identification can impact our knowledge of the internal composition and dynamics of these bodies as well as their potential habitability.

1 Introduction

Ammonia is an important anti-freezing molecule (Neveu et al., 2017) and the identification of ammonium minerals on the surface of planetary bodies might provide important evidence of the interaction between the inside (oceans/brines) and outside (surface) of these bodies, indicative of a young and renewed surface (Loeffler et al., 2010). As on Earth, NH_4^+ minerals are ancillary phases and not always straightforward to interpret from remote sensing data. There are several icy bodies inside the Solar System, where planetary space missions have discovered ammonium-bearing minerals (e.g., Ceres), whereas in others (e.g., Pluto system) their presence has just been presumed due to difficulties in their identification. Recently, on the asteroid Ryugu, the presence of NH-rich material was presumed in relation to the similarities of the 3.05 μm absorption bands with the spectrum of Ceres. (Pilorget et al., 2021).

Ceres' surface was investigated by the *Dawn* mission that performed near-global geological, chemical, and geophysical mapping of this body. For the first time, King et al., (1992) detected ammonium compounds on Ceres' surface focusing in the 3 μm spectral range. De Sanctis et al., 2020 suggested that the presence of ammonium bicarbonate and/or ammonium chlorides on Ceres' surface is a residual of the recent ascent of deep brine in agreement with some authors (e.g., Castillo-Rogez, 2020) that proposed the existence of an early ocean in the subsurface of Ceres as deep brine. Data collected by the *Dawn* mission also evidenced the presence of NH_4^+ phyllosilicate materials (Russell and Raymond, 2011; De Sanctis et al., 2015). The spectral fit of VIR data coming from the bright *faculae* in the Occator area, is well solved by including ammonium salt salammoniac (NH_4Cl) and ammonium carbonate $(NH_4)_2CO_3$ as the best candidates given the absorption bands located at 2.2 μm (De Sanctis et al., 2016). The genesis of these salts is linked to the existence of water fluid and hydrothermal activity (De Sanctis et al., 2016). The surface liquid is attributed to two different phenomena: (i) heating of surface after impacts, and (ii) early inner fluids that interact with the surface through cryovolcanism phenomena, coming outside from fractures (De Sanctis et al., 2020).

Several icy worlds have been discovered inside the Solar System, together with Ceres, Pluto and its moon Charon, they are also considered to be icy bodies. Pluto is a Trans-Neptunian Object located in the Kuiper Belt probably originated from an impact that could have also generated its five satellites: Charon, Styx, Nix, Kerberos, and Hydra (Stern et al., 2006). Cryovolcanism processes can be active on moderately large but very cold objects. Virgil Fossae on Pluto shows evidence of recent cryovolcanism activity and ammonia signature (Cruikshank et al., 2019), based on data collected by the Linear Etalon Imaging Spectral Array (LEISA) installed in the *New Horizons* mission (Schmitt et al., 2017, Dale Ore et al. 2019). Ammonium minerals NH_4Cl and $(NH_4)_2CO_3$, might explain the absorption bands located in the 2.15-2.17 μm range (Cruikshank et al., 2019); whereas Dalle Ore et al. (2019) identify ammonia (NH_3) through the absorption bands located at 1.65 and 2.21 μm. These observations suggest the presence of subsurface liquids and the most recent models are created taking into account the presence of an internal ocean on Pluto (Kimura and Kamata, 2020).

Charon is Pluto's largest natural satellite, is icier than Pluto, and has interesting extensional tectonic surface features that are consistent with the possible existence of an ancient internal ocean (Beyer et al., 2018). Ammonium chloride, ammonium nitrate, and ammonium carbonate are selected as the most important candidate minerals to represent the surface of Charon, giving the abundance of N, C, and O in the Pluto system (Cook et al., 2018). A possible theory for the presence of ammonia on Charon surface is the hauling out from subsurface local concentration of NH_3 after impacts (Grundy et al., 2016). Pluto's smaller satellites, Nix and Hydra, also show absorption bands at 2.21 μm

associated with ammoniated species (Cook et al., 2018), thus, the whole Pluto system seems to contain NH_4^+ compounds.

A larger and slightly hotter object such as Titan, the largest moon of Saturn, is likely differentiated into several layers with a rocky core surrounded by other levels composed of different crystalline forms of ice. A liquid layer, a sort of "*magma*" made of water and ammonia could be present between the crust and a deeper ice layer composed of hexagonal ice and high-pressure forms of ice, respectively (Fortes, 2000). The likely occurrence of a liquid layer in the interior of Saturn might be the result of the presence of ammonia that allows water to remain liquid even at a temperature as low as 176 K (Hammond et al., 2018). Fortes et al., 2007 modelled the crustal bedrock of Titan as a mixture of methane clathrate, ice, and ammonium sulfates $(NH_4)_2SO_4$, which can erupt in the form of brines on the surface.

Ammonium compounds are also present on the evolved telluric planets. On Mars, in the Iani Chaos area, absorption bands at 1.07, 1.31, and 1.57 μm are identified as ammonium sulfates mascagnite $(NH_4)_2SO_4$ and letovicite $(NH_4)_3H(SO_4)_2$ (Sefton-Nash et al., 2012). Quinn et al., (2011) report the ammonium detection in the Phoenix landing site soil at a concentration of 0.86×10^{-7} mole NH_4^+ cm^{-3}.

On Earth, nitrogen is present in rocks as recalcitrant organic matter and possibly in mantle rocks, either as ammonium/nitrate salts, or as fixed NH_4^+ in silicate minerals (clay, mica, feldspar, etc.) (Holloway and Dahlgren, 2002, Mysen, 2019). NH_4^+ silicate minerals are formed by replacing potassium with ammonium, leading to a small re-organization of the mineral crystal structure (Holloway and Dahlgren, 2002). Ammonium-bearing minerals, occurring in fumarolic, hydrothermal systems, and active/fossil hot-springs sites, are rare but can be important as markers of such past environmental conditions in the localities where they were found (Balić-Žunić et al., 2016a;b).

Ammoniated compounds are also present in primordial bodies such as comets. Recently, Poch et al. (2020) compared the spectrum of the comet 67P with several NH_4^+ salts in the spectral range from 3 to 3.5 μm concluding that they are probably the best candidates, not excluding the presence of some organics, to fit the band located at 3.2 μm in the comets' spectrum. Altwegg et al. (2020) also report the detection of ammonium-bearing minerals from a dust grain that collided with the Rosetta spacecraft while it orbited the Comet 67P. NH_4^+ salts are of great interest because they could carry a large fraction of the nitrogen present in the form of semi-volatile solids in comets, thus solving the problem of their low nitrogen-to-carbon ratios (Poch et al. 2020, Nuth III et al., 2020). The identification of ammonium compounds on the solar system objects is mostly made through the identification of absorption bands in the near-infrared reflectance spectra of their surface. But only a limited number of laboratory studies are devoted to the study of these compounds in the visible and near-IR ranges.

Early studies on ammonium minerals were carried out by Krohn and Altaner (1987) on a set of NH_4^+ clays and sulfates in the spectral range from 0.5 to 2.5 μm, and by Bishop et al. (2002) on clay minerals and altered tephra analyzed in the spectral range from 1 to 7 μm. Recently, Berg et al. (2016) reported reflectance spectra up to 8 μm for a wide set of ammoniated salts, whereas Ferrari et al. (2019) analyzed a group of ammonium-bearing phyllosilicates to study the NH_4^+-carrier phases detected on Ceres. Poch et al. (2020) specifically studied the 3-4 μm range of a series of NH_4^+ compounds for their identification at the surface of comets and asteroids.

Notwithstanding the large literature on ammoniated minerals, the effects of low temperature (*T*) as well as those of grain size on the reflectance spectra are not considered by many authors (Ehlmann et al., 2018). In this work, we measured and analyzed a set of natural terrestrial analogs and synthetic NH_4^+ salts of interest for planetary science in the spectral range from 1 to 5 μm down to 60K. We also study the effect of texture by measuring three different grain sizes (32-80 μm, 80-125 μm, 125-150 μm) at room *T*. This study focuses on understanding the role of different anionic groups (sulphates, phosphates, aluminates, and borates), degree of hydration, and crystal-chemical features on the structure of the near-infrared spectra of ammonium compounds. It also assesses how external parameters such as temperature, which can also trigger phase changes, and grain size affect the reflectance spectra of the selected samples.

The collected cryogenic data, with a special focus on the NH_4^+ absorption bands, can be used for the detection of these collected salts on Pluto's surface as well as on other planetary bodies such as icy satellites, asteroids, Kuiper Belt Objects (KBOs) and comets. The presence and the crystal-chemical modifications (e.g., phase transformations) of NH_4^+ minerals in the ice shell of icy satellites might influence their internal dynamics. Therefore, as well as the composition of the non-ice components and their evolution beneath an icy planet's crust is a fascinating subject that allows speculating about the thickness of the icy crust (Comodi et al. 2014, Comodi et al., 2017), as well the composition of the oceans and/or the presence of localized brine area underneath the crust.

NH_4^+ spectral properties

The fundamental vibrational modes of the NH_4^+ group in ammonium minerals are located at: ~3.25-3.30 μm for the ν_1 symmetric stretch, ~5.7-5.95 μm for the ν_2 in-plane bend, ~3.0-3.23 μm for the ν_3 asymmetric stretch and ~6.7-7.2 μm for the ν_4 out-of-plane bend. The vibrational modes around 3.3 and 5.8 μm are only Raman active, whereas the latter two near 3.2 and 7 μm are IR and Raman active (Krohn, and Altaner, 1987, Bishop et al 2002). As reported by Berg et al. (2016), the absorption bands between 3 and 4 μm can also be attributed to the NH_4^+ overtones and combinations, the bands at ~ 3.23 - 3.33 μm can be attributed to the $\nu_2+\nu_4$ mode and at ~ 3.57 μm to the $2\nu_4$ overtone mode. Near 1.05, 1.3 and 1.56 μm absorption bands respectively due to the $3\nu_3$ overtone, the $2\nu_3+\nu_4$ combination and the $2\nu_3$ overtone are located with some possible contributions from the $\nu_1+\nu_3$ combination. At 2.0-2.1 μm absorption bands can be assigned to the $\nu_2+\nu_3$ and $\nu_1+\nu_4$ combination modes (Bishop et al., 2002). In addition to the vibrational modes listed above, ammonium chloride exhibits triply degenerated vibrational modes ν_6 (IR active) and a transverse-optic mode ν_{5TO} (IR and Raman active) (Schumaker and Garland, 1970).

2 Materials and methods

Samples

Nine ammonium-bearing salts were analyzed, considering both (i) natural and (ii) synthetic salts (Tab. 1).

(i) The natural samples were preliminarily characterized at the Department of Physics and Geology, University of Perugia (Italy), using X-ray powder diffraction (XRPD). XRPD measurements were carried out by means of a Philips PW 1830 diffractometer, with a graphite monochromator, and using the CuK_α radiation (λ = 1.54184 Å). Data were taken with a step scan of 0.02 °/step and a step time of 100 s/step. Quantitative measurements of the collected data were carried out using the Rietveld refinement method (Rietveld, 1969), as implemented in the EXP-GUI GSAS software (Larson and Von Dreele, 1988; Toby, 2001). Details on the X-ray powder diffraction measurements and quantitative analyses can be found in Guidobaldi et al. (2018).

(ii) The synthetic salts were purchased on the market and certified with >98% purity. All the samples were first finely ground with an agate mortar and then sieved in three different granulometry size ranges (32-80 µm, 80-125 µm, 125-150 µm). Grain sizes were chosen as a representative dimension of the granular materials present on the surface of planetary bodies.

Table 1: Compositional data, source and description for selected samples used in this study.

Mineral name	Chemical formula	Source/description
Ammonium sulphate / mascagnite	$(NH_4)_2SO_4$	Pozzuoli, Italy – XRPD checked: small amount of mohrite 6.4%
Ammonium chloride / salammoniac	NH_4Cl	Pozzuoli, Italy – XRPD checked: 100%
Larderellite	$(NH_4)B_5O_7(OH)_2 \cdot H_2O$	Larderello, Italy – XRPD checked: small amount of bassanite 0.4% and polyhalite 5.4%
Struvite	$(NH_4)MgPO_4 \cdot 6(H_2O)$	Limfjord, Denmark – XRPD checked: 100%
Tschermigite	$(NH_4)Al(SO_4)_2 \cdot 12(H_2O)$	Cermniky, Czech Republic – XRPD checked: 100%
Ammonium carbonate	$(NH_4)_2CO_3$	Synthetic, Acros Organics > 98%
Ammonium phosphate monobasic	$(NH_4)H_2PO_4$	Synthetic, Carlo Erba > 98%
Ammonium nitrate	NH_4NO_3	Synthetic, Panreac AplliChem > 99%
Ammonium bicarbonate	$(NH_4)HCO_3$	Synthetic, Carlo Erba > 98%

Reflectance measurements

Reflectance spectra were collected at the Institut de Planétologie et d'Astrophysique de Grenoble (IPAG) (France), with the SHINE Spectro-Gonio Radiometer (Brissaud et al., 2004) of the Cold Surface Spectroscopy (CSS) facility (https://cold-spectro.sshade.eu). The instrument is a homemade

bidirectional VIS-NIR reflectance spectrometer, which we used to measure the reflectance spectra over the whole 1–4.8 μm spectral range. A spectral sampling of 10 nm was used up to 3.2 μm and 20 nm above with effective spectral resolution varying in 3 steps (3 gratings with fixed slit width) between 7.5 to 30 nm over the range. The sample was illuminated at a fixed geometry (incidence 0°, emergence 20°) with a spot of monochromatic light of approximately 7.5 mm in diameter. Spectralon© and Infragold© targets were used as standard references, measured at room *T* and radiometrically characterized in terms of BRDF. The instrument is equipped with a cryogenic simulation chamber, CarboN-IR, to control the temperature of the minerals. Spectra were measured at different temperatures (typically 10-20 spaced by 10-25K steps) ranging from 298 K to a minimum temperature varying between 90 and 62 K depending on samples. For samples with a phase transition in this range a series of 7-9 additional spectra were taken at 1 K steps around the transition *T*, both during cooling and warming to monitor the phase transition. The samples to be measured (between 0.15 and 0.45 g of powder) were put in an aluminum sample holder cup, 12-16 mm in diameter and 3-4 mm deep. The density and porosity of the samples were calculated using the measured sample volume and mass and the bulk density of the mineral. They range between 0.40-0.80 g/cm^{-3} and 58-78%, respectively. The sample holder was placed in a closed copper cell isothermally cooled with a He-cryostat and equipped with large optical access through two sapphire windows. Nitrogen was kept in the closed isothermal cell to allow an excellent thermal equilibrium of the fine and porous powders. This internal cell was placed inside an external chamber, in which a high vacuum (~10^{-5} mb) is performed. This configuration allowed the collection of reflectance spectra at temperatures down to 60 K with a sample powder temperature homogeneity and accuracy better than 1 K.

Data reduction

The measured spectra were first calibrated using the measurements of the Spectralon© and Infragold© reference targets and the standard calibration procedure of the instrument with an additional photometric correction taking into account the contribution of the two optical windows under our observation conditions (i=0°, e=20°).

The data analyses were then carried out in several steps. For each absorption band, the continuum removal range was kept constant for all the analyzed spectra. The position of the absorption bands was then computed using a second-order polynomial fit around the minimum. The band depth was determined using the Clark and Roush (1984) equation: $D = (R_c - R_b)/R_c$ where R_b is the reflectance at the band center and R_c is the reflectance of the continuum at the band center. The band area was computed by numerical integration over the band. The width (FWHM) was computed by intersecting the continuum-removed band with a horizontal line passing at the half depth. For those spectra showing band complexes with multiple minima, the spectral continuum was computed between the two shoulders of the band complex, and the position of every single minima were fitted with a second-order polynomial. The band area and depth were computed for the entire band complex and not for all relative minima. Details on the data reduction procedures can be found in Comodi et al. (2021). The spectral reduction was performed only on absorption bands of interest for remote sensing identification which are located at ~1.05, ~1.3, ~1.56, ~2.02, and ~2.2 μm.

3 Results

3.1 Common spectral bands

The reflectance spectra of the natural and synthetic samples acquired at room *T* are reported in Figure 1. The spectra of natural samples acquired at low *T* are reported in Figure 2 (with different grain

sizes), while the spectra of synthetic compounds are reported in Figure 3 (with different grain sizes). Table 2 provides the absorption bands positions at room temperature and their assignment. The collected spectra are characterized by several spectral features and evolutions with *T* which are common for all the samples. In particular, among the numerous absorption bands occurring in the range of 1 to 5 μm, most of them are due to the NH_4^+ group.

NH_4^+ overtone and combination bands take place at ~1.05, ~1.3, ~1.56, ~2.02, and ~2.2 μm at room *T*. Between ~2.8 and 3.8 μm multiple NH_4^+ features are evident but not always clearly identifiable. See Table 2 for detailed band assignments. Absorption bands located at ~1.47, ~1.94, ~2.62, and ~2.83 μm are due to the presence of some water absorbed in the grains before the measurements. This is due to the high hygroscopic nature of some of the selected samples. The bands related to water vibrational modes appear even with very small amounts of absorbed or adsorbed H_2O due to their high absorption coefficient (Salisbury and Walter, 1989; Pommerol et al., 2009) and are emphasized at low *T*. Several absorption bands appear over 3μm, in anhydrous samples, confirming the presence of water absorbed in the grains. The nominally anhydrous samples were placed in a desiccator chamber with reduced humidity days prior to the measurements, and only a few additional minutes passed between the extraction of the sample powder and its insertion into the cell purged with dry N2 for analysis.

The collected low *T* spectra reveal fine structures displaying more specific and defined absorption bands compared to the room *T* ones (De Angelis et al., 2019; De Angelis et al., 2021). Moreover, the reflectance spectra of the hydrated samples show saturated and featureless spectra above 3 μm, a region dominated by the very strong and broad H_2O absorption bands (Clark et al., 1990). Hydrated NH_4^+ salts display the typical water bands around ~1.4, ~1.9, and 3 μm with additional weaker overtone and combination bands at ~1.2 and ~1.75 μm (Krohn, and Altaner, 1987, Bishop et al 2002). The latter two bands are not attributed as they overlap with those of NH_4^+. The NH_4^+ vibrational modes characterize the spectra of the selected ammonium minerals; however, spectral differences are expected as a function of different hydrogen bonds and cation types (Comodi et al., 2021). The discontinuity in the spectra between 4.20-4.32 μm, which has not been recorded, is related to the strong absorption of the atmospheric CO_2 gas.

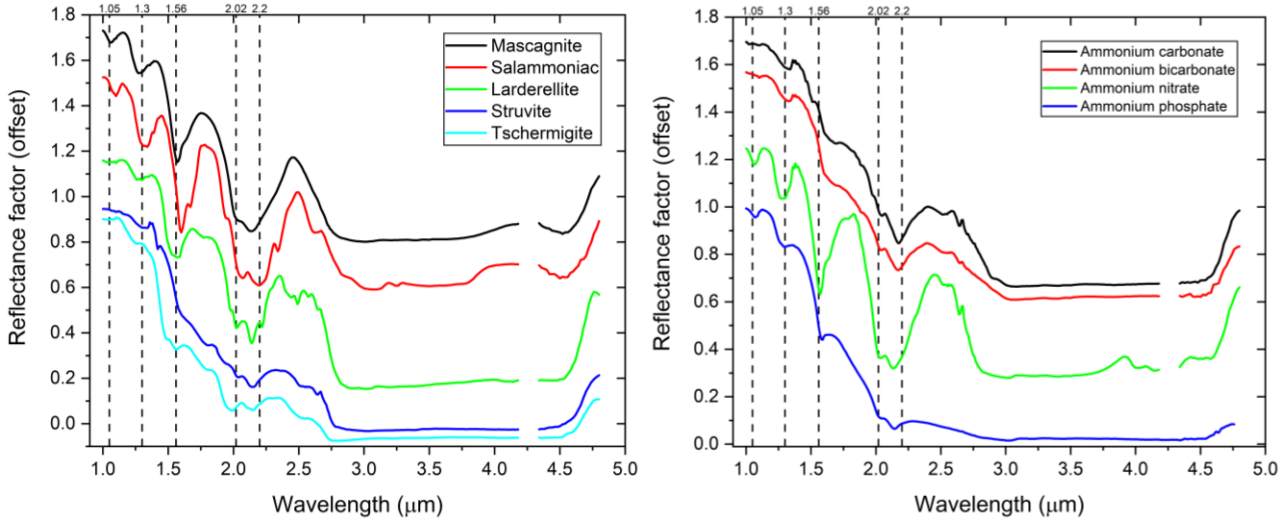

Fig.1: Reflectance spectra of natural (left) ammonium-bearing minerals mascagnite (black), salammoniac (red), larderellite (green), struvite (blue), and tschermigite (light blue) and synthetic compounds (right) ammonium carbonate

(black), ammonium bicarbonate (red), ammonium nitrate (green), ammonium phosphate (blue) at room temperature (TAMB). The spectra have been offset vertically for clarity. The vertical dotted lines mark the five bands analyzed in this work. The discontinuity in the spectra between 4.20-4.32 μm is related to the strong absorption of the atmospheric CO_2 gas

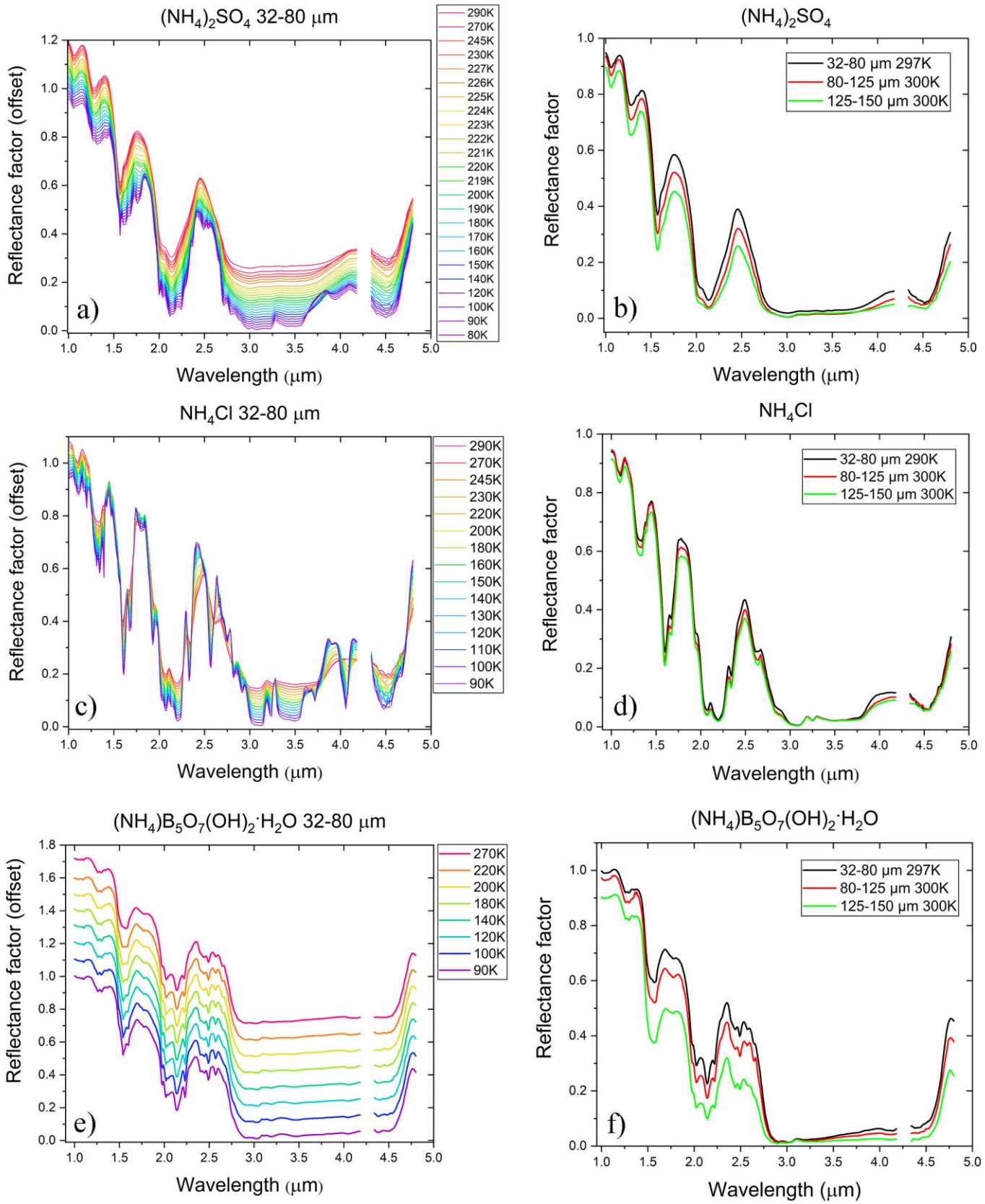

Fig.2: (continued)

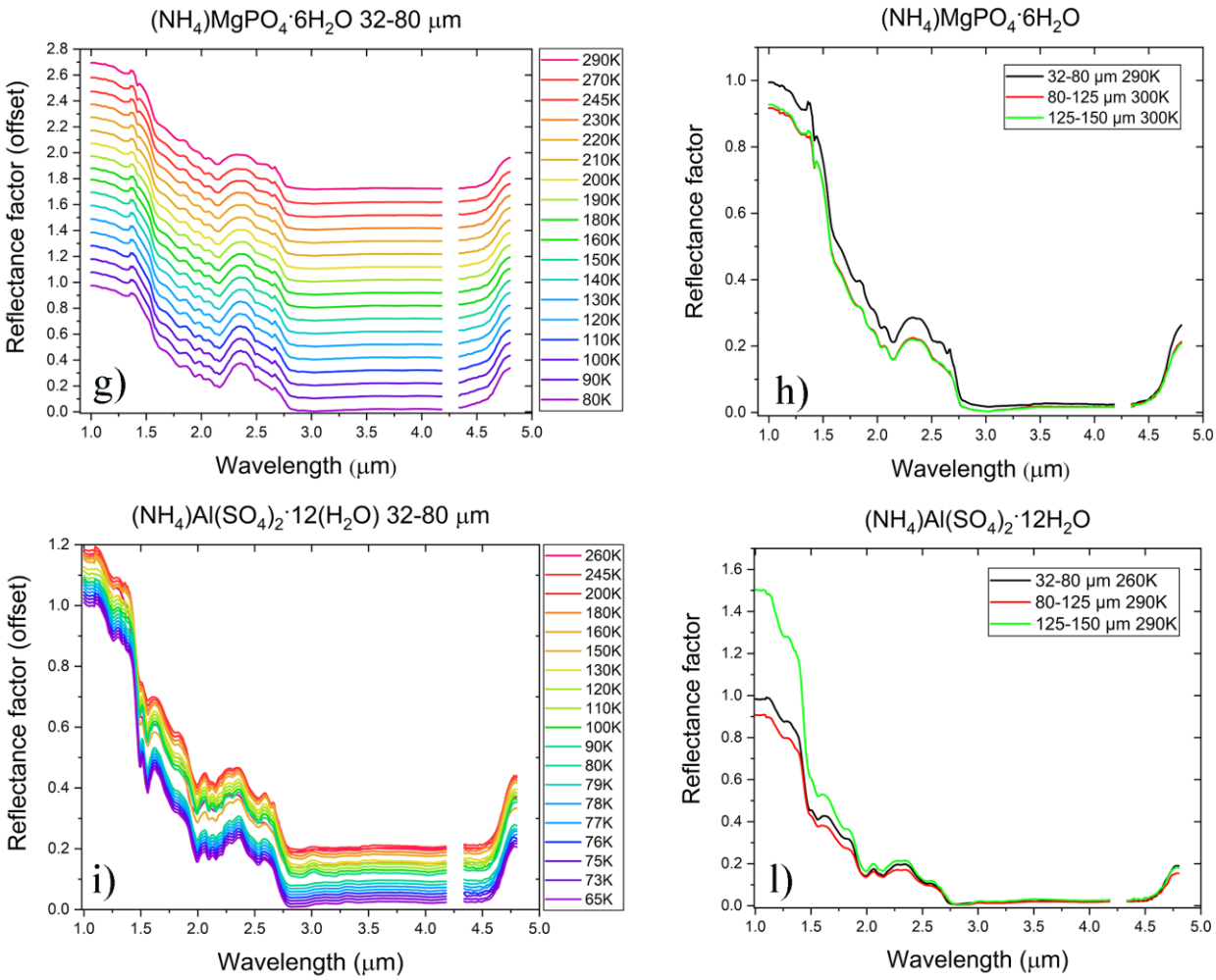

Fig.2: Low-temperature reflectance (1-4.8 μm) spectra of the natural samples. Left panels: (a) $(NH_4)_2SO_4$ (mascagnite) spectra of 32-80 μm powder down to 80K. (c) NH_4Cl (salammoniac) spectra of 32-80 μm powder down to 90K. (e) $(NH_4)B_5O_7(OH)_2{\cdot}H_2O$ (larderellite) spectra of 32-80 μm powder down to 90K. (g) $(NH_4)MgPO_4{\cdot}6(H_2O)$ (struvite) spectra of 32-80 μm powder down to 80K. (i) $(NH_4)Al(SO_4)_2{\cdot}12(H_2O)$ (tschermigite) spectra of 32-80 μm powder down to 65K. The spectra have been offset vertically for clarity. Right panels: (b;d;f;h;l) reflectance spectra collected at room temperature for the three different grain sizes (black 32-80 μm; red 80-125 μm; green 125-150 μm) for the same samples. The discontinuity in the spectra between 4.20-4.32 μm is related to the strong absorption of the atmospheric CO_2 gas

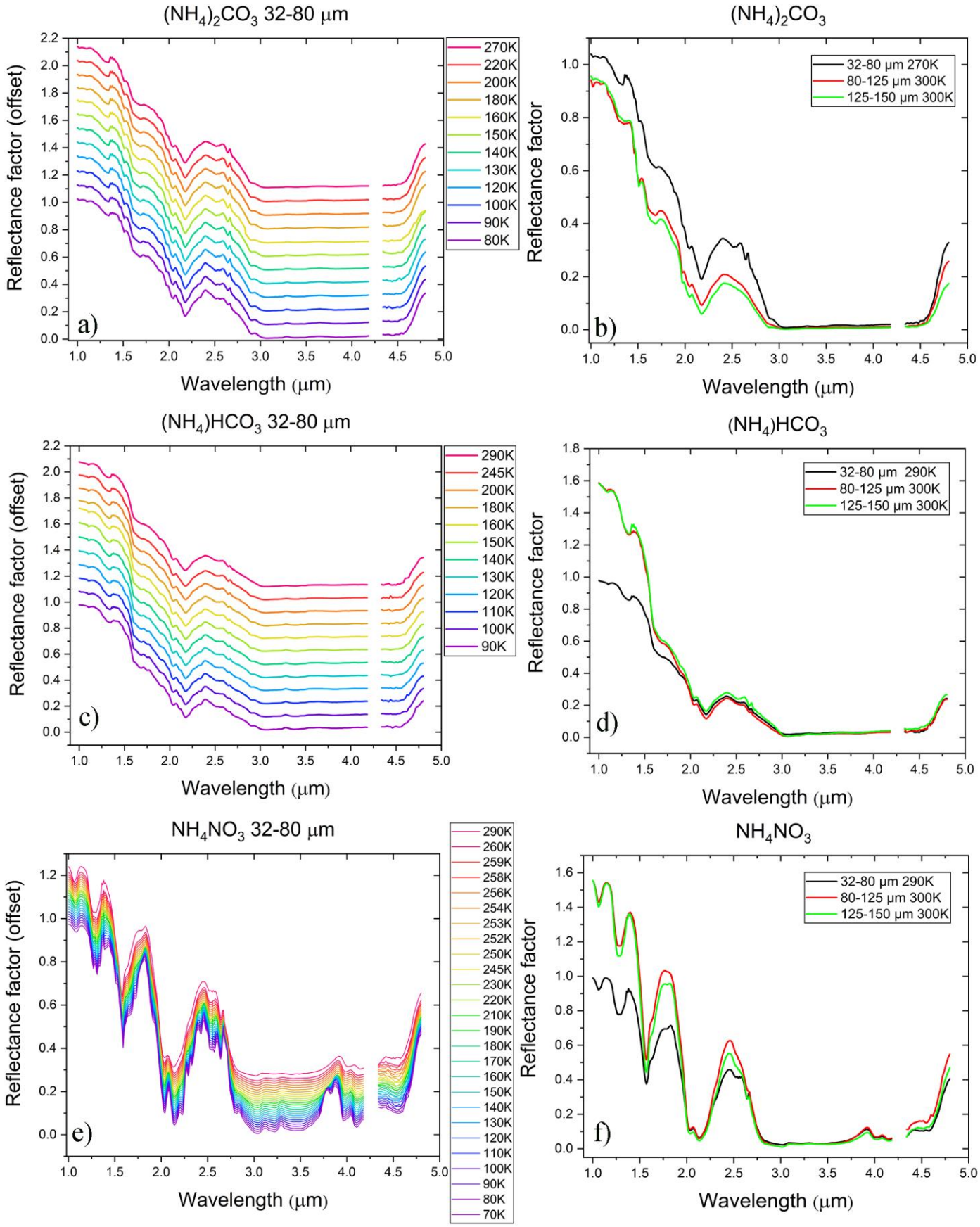

Fig.3: (continued)

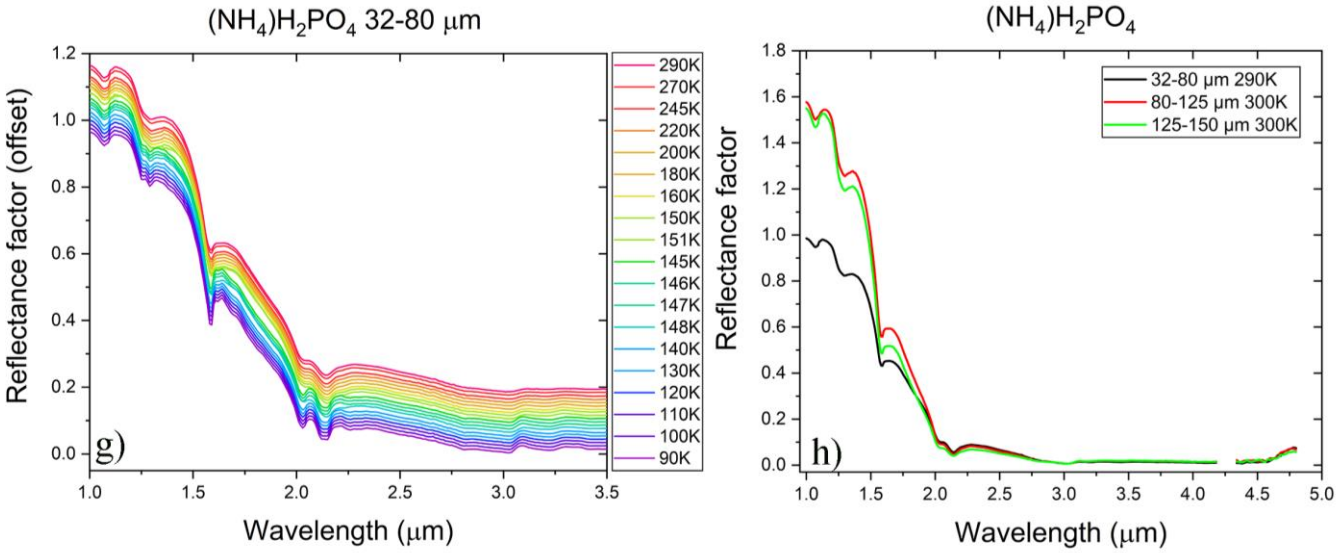

Fig.3: Low-temperature reflectance spectra (1-4.8 µm) of synthetic samples. Left panels: (a) $(NH_4)_2CO_3$ (ammonium carbonate) spectra of 32-80 µm powder down to 80K. (c) $(NH_4)HCO_3$ (ammonium bicarbonate) spectra of 32-80 µm powder down to 90K. (e) NH_4NO_3 (ammonium nitrate) spectra of 32-80 µm powder down to 70K. (g) $(NH_4)H_2PO_4$ (ammonium phosphate) 1-3.7 µm spectra of 32-80 µm powder down to 90K. The spectra have been offset vertically for clarity. Right panels: (b;d;f;h) reflectance spectra collected at room temperature of the three different grain sizes (black 32-80 µm; red 80-125 µm; green 125-150 µm) for the same samples. The discontinuity in the spectra between 4.20-4.32 µm is related to the strong absorption of the atmospheric CO_2 gas

Table 2: Absorption band positions of reflectance spectra collected at room temperature. Band assignments were made following: (1) Berg et al 2016, (2) Fastelli et al., 2020, (3) Stefov et al., 2004, (4) Sergeeva et al., 2019 and (5) Cloutis et al., 2016, (6) Schumaker and Garland, 1970

Mineral	Band Positions (µm)	Vibrational modes
Mascagnite[1] $(NH_4)_2SO_4$	1.06	NH_4^+ $3\nu_3$
	1.28	NH_4^+ $2\nu_3 + \nu_4$
	1.58(I) 1.64(II)	NH_4^+ $2\nu_3$
	2.02	NH_4^+ $\nu_2 + \nu_3$
	2.18	NH_4^+ $\nu_3 + \nu_4$
	3.01	NH_4^+ ν_3
	3.21[u]	NH_4^+ $\nu_2 + \nu_4$
	3.40[u]	NH_4^+ $2\nu_4$
	3.50[u]	NH_4^+ $2\nu_4$
	~4.5	SO_4^{2-} overtones and combinations
Salammoniac[1,6] NH_4Cl	1.09	NH_4^+ $3\nu_3$
	1.32 (I) 1.38 (II)	NH_4^+ $2\nu_3 + \nu_4$
	1.47[u]	H_2O $2\nu_2 + \nu_3$
	1.62(I) 1.67 (II)	NH_4^+ $2\nu_3$
	1.94	H_2O $\nu_2 + \nu_3$
	2.06	NH_4^+ $\nu_2 + \nu_3$
	2.20(I) 2.33 (II)	NH_4^+ $\nu_1 + \nu_4$ and/or NH_4^+ $\nu_3+\nu_4$
	2.62	NH_4^+ $\nu_3 + 2\nu_6$ and/or OH ν_3
	2.83	NH_4^+ $\nu_3 + \nu_6$ and/or H_2O ν_3
	3.05	NH_4^+ ν_3
	3.24[u]	NH_4^+ $\nu_2 + \nu_4$

	~3.5[u, w] 3.72 4.5	NH_4^+ $2\nu_4$ NH_4^+ $\nu_2 + 2\nu_6$ NH_4^+ $\nu_2 + \nu_6$ and H_2O $\nu_2 + \nu_{L2} + \nu_{T2}$
Larderellite[2] $(NH_4)B_5O_7(OH)_2 \cdot H_2O$	1.05 1.25(I) 1.28(II) 1.34(III) 1.55 1.76 1.97 2.03 2.14 2.23 2.45(I) 2.50(II) 2.57 2.9 3.01[u] 3.20[u] 4.17[u]	NH_4^+ $3\nu_3$ NH_4^+ $2\nu_3 + \nu_4$ NH_4^+ $2\nu_3$ / H_2O OH H_2O $\nu_2 + \nu_3$ NH_4^+ $\nu_2 + \nu_3$ / H_2O $\nu_2 + \nu_3$ NH_4^+ $\nu_3 + \nu_4$ NH_4^+ $\nu_3 + \nu_4$ NH_4^+ $2\nu_3$ OH ν_3 H_2O ν_3 NH_4^+ ν_3 / H_2O ν_1 NH_4^+ $\nu_2 + \nu_4$ / H_2O ν_1 BO_3 / BO_4 combinations
Struvite[3] $(NH_4)MgPO_4 \cdot 6H_2O$	1.29 1.42 1.65[u] 1.80 1.91 2.03 2.13 2.51 2.64 2.8	NH_4^+ $2\nu_3 + \nu_4$ NH_4^+ $2\nu_3$ / OH 2ν NH_4^+ $\nu_2 + \nu_3$ NH_4^+ $\nu_2 + \nu_3$ / H_2O $\nu_2 + \nu_3$ NH_4^+ $\nu_3 + \nu_4$ NH_4^+ $2\nu_3$ H_2O ν_3
Tschermigite[4] $(NH_4)Al(SO_4)_2 \cdot 12H_2O$	1.22 1.48 1.51 1.75 1.98 2.10 (I) 2.14(II) 2.30 2.49 2.75	NH_4^+ $2\nu_3 + \nu_4$ NH_4^+ $2\nu_3$ / OH 2ν NH_4^+ $\nu_2 + \nu_3$ NH_4^+ $\nu_2 + \nu_3$ / H_2O $\nu_2 + \nu_3$ NH_4^+ $\nu_3 + \nu_4$ NH_4^+ $\nu_3 + \nu_4$ NH_4^+ $2\nu_3$ H_2O ν_1
Ammonium carbonate[1] $(NH_4)_2CO_3$	1.09 1.28 1.45 1.50 1.64 2.03 2.20 2.50 2.63 3.06[u]	NH_4^+ $3\nu_3$ NH_4^+ $2\nu_3 + \nu_4$ NH_4^+ $2\nu_3$ NH_4^+ $\nu_2 + \nu_3$ NH_4^+ $\nu_3 + \nu_4$ CO_3^{-2} $\nu_1 + 2\nu_3$ OH ν_3 NH_4^+ ν_3
Ammonium phosphate[1] $(NH_4)H_2PO_4$	1.07 1.28 1.57 2.02 2.14 3.02 3.20[u]	NH_4^+ $3\nu_3$ NH_4^+ $2\nu_3 + \nu_4$ NH_4^+ $2\nu_3$ NH_4^+ $\nu_2 + \nu_3$ NH_4^+ $\nu_3 + \nu_4$ NH_4^+ ν_3 NH_4^+ $\nu_2 + \nu_4$

Ammonium nitrate[5] NH_4NO_3	1.07 1.28 1.57(I) 1.64(II) 1.78 2.02 2.14 2.52 2.63 3.02 3.21[u] 3.40 3.49[u] 4.02 4.14 ~4.50	NH_4^+ $3\nu_3$ NH_4^+ $2\nu_3 + \nu_4$ NH_4^+ $2\nu_3$ NH_4^+ $\nu_2 + \nu_3$ NH_4^+ $\nu_2 + \nu_3$ NH_4^+ $\nu_3 + \nu_4$ OH ν_3 OH ν_3 NH_4^+ ν_3 NH_4^+ $\nu_2 + \nu_4$ NH_4^+ $2\nu_4$ NH_4^+ $2\nu_4$ NO_3^- NO_3^- NO_3^- $\nu_3 + \nu_2$
Ammonium bicarbonate[1] $(NH_4)HCO_3$	1.09 1.30 1.62 1.88 2.03 2.19 2.54 2.64 3.20[u] 3.38[u] 3.50[u] ~4.5	NH_4^+ $3\nu_3$ NH_4^+ $2\nu_3 + \nu_4$ NH_4^+ $2\nu_3$ H_2O $\nu_2 + \nu_3$ NH_4^+ $\nu_2 + \nu_3$ OH ν_2 CO_3^{-2} $\nu_1+2\nu_3$ OH ν_3 NH_4^+ $\nu_2 + \nu_4$ NH_4^+ $2\nu_4$ (?)

u: uncertain band, the position is approximate because bands can be assigned also to the presence of hygroscopic water

.

3.2 Natural samples spectral features

Mascagnite $(NH_4)_2SO_4$ reflectance spectra are reported in Fig.2a down to 80K. The overall reflectance spectra of this sample, compared to the salammoniac one, shows a decreased and less defined number of absorption bands as reported by Berg et al. (2016). NH_4^+ absorption bands are located near 1 μm, at ~1.56 μm, and ~2.2 μm. Above 3 μm absorption bands become broad and saturated resulting in uncertain band positions. The fundamental vibrational modes of SO_4^{2-} are located at 9.6–10.4 μm for ν_1, at 19–24 μm for ν_2, at 7.8–10.4 μm for ν_3 and 13–18 μm for ν_4 (Ross, 1974). Combinations and overtones of these modes are located in the 4-5 μm region (Cloutis et al., 2006) partly affected in our spectra by the CO_2 gas band (4.20-4.32μm). At the critical temperature (T_c) of 223K, ammonium sulfate is characterized by a phase transition, defined as ferroelectric transition, with a change in space group from *Pnma* at room *T* to *Pna*2_1 at low *T* (Schlemper and Hamilton, 1966). The phase transition generates changes in the spectrum at ~1.8 μm and at ~ 2.6 μm (figure 2a yellow spectra). The spectra of the three different grain sizes (Fig. 2b) show deeper and generally more defined bands when increasing granulometry. The reflection peaks in the ~ 1–1.6 μm range are higher for the coarse grain size.

Reflectance spectra of **salammoniac NH_4Cl** are reported in Fig. 2c down to 90K. Numerous absorption bands occur in the range from 1 to 4.8 μm, most of them are due to NH_4^+ groups. NH_4^+ overtone and combination take place at ~1.05, ~1.3, ~1.56, ~2.02, and ~2.12 μm at room T. Salammoniac also shows distinct absorption bands at 1.09, 1.33, 1.38 1.62 and 1.67 μm, three bands in the ~2-2.4 μm range and a complex of absorption features between 3.0 and 3.8 μm with several saturated bands. In the 3.2 – 3.3 μm spectral range doublet peaks appear at low *T* as other chloride minerals collected in the same conditions (De Angelis et al., 2022). Salammoniac undergo a phase transition at T_c 242K, defined as an order-disorder transition because of the rearrangement of hydrogen bonds (Levy and Peterson, 1952). Above T_c, the mineral displays a disordered CsCl-type crystal structure in which the NH_4^+ ions are arbitrarily distributed between two energetically equivalent orientations (Wang and Wright, 1972). For this reason, below T_c, at ~1.8 μm, 2.5-2.95 μm and 3.6-4.2 μm the absorption bands drastically change (Fig. 2c orange spectra). Details in the spectral behavior below the phase transition are reported in the discussion section. All the absorption bands described above are also present in the spectra of the other two granulometries (80-125 and 125-150 μm) (Fig. 2d).

Larderellite $(NH_4)B_5O_7(OH)_2 \cdot H_2O$ spectra (Fig. 2e), collected down to 90K, show absorption bands assigned to NH_4^+ overtones and combinations overlapped to those of H_2O and OH group at 1.55, 2.03, 3.01, 3.20 and 4.14 μm (positions referred to ambient *T* spectra). H_2O and OH absorption bands are identified at 1.55, 1.76, and 1.97 μm. The complex band near 2.2 μm is due to NH_4^+ overtone and combination modes. In the spectral range above 3 μm, bands are broad (~3.01, ~3.20, and ~4.14 μm) and of uncertain attribution due to the presence of water molecules. Spectra of this sample at different granulometry are reported in Fig. 2f with no evident change in the band shapes.

The reflectance spectra of **struvite $(NH_4)MgPO_4 \cdot 6H_2O$** (Fig. 2g) and **tschermigite $(NH_4)Al(SO_4)_2 \cdot 12H_2O$** (Fig. 2i) collected down to 80K and 65K, respectively, are characterized by a reduction in the number of spectral features due to the presence of six and twelve water molecules w, respectively. Most of the water bands overlapped and combined with the NH_4^+ vibrational modes and increased the complexity of the spectra. For this reason, the bands became less deep and defined and the high amount of water generates a low reflectance level where the NH_4^+ bands are strongly blended, vibrational coupling occurs. With decreasing temperature, the H_2O bands became narrower

and more defined due to a strengthening of hydrogen bonding. In the room *T* spectra, the strong water absorption bands saturated the 3 μm region. In the struvite mineral, NH_4^+ modes are located at 1.29, 1.65, 2.04, 2.15, 2.51, and 2.64 μm, whereas in tschermigite they are at 1.22, 1.75, ~2.12, 2.30, and 2.49 μm.

Tschermigite, in the investigated temperature range, underwent a phase transition at T_c ~77K, from para- to ferroelectric phase where the sulfate groups are ordered by the crystallographic direction [111] becoming the polar axis (Korchak at al., 2007; Bohmer et al., 1990; Sekine et al., 1988).

3.2 Synthetic samples spectral features

Reflectance spectra of the two NH_4^+carbonates, **ammonium carbonate $(NH_4)_2CO_3$** (Fig. 3a) and **ammonium bicarbonate $(NH_4)HCO_3$** (Fig. 3c) are characterized by the presence of NH_4^+ overtone and combination bands in the spectral range below 2.5 μm. Their spectral features were consistent with those presented in the literature (Berg et al., 2016) with the complete saturation of the CO_3^{2-} vibrational modes in the 3-4 μm area due to the high hygroscopicity of these salts. The CO_3^{2-} fundamental modes occurred at 9.4 μm (ν_1), 11.37 μm (ν_2), 7.06 μm (ν_3) and 14.7 μm (ν_4) (Frost and Palmer, 2011). The main combination bands of this group can be found in the 3.4 - 4.0 μm range (Zhu et al., 2020). Ammonium carbonate and bicarbonate spectra are quite similar and show the same behaviour on decreasing temperature, but small spectral variations were possibly due to different degrees of hydrogen bonds (Berg et al., 2016). These similarities between spectra can also be attributed to the high hygroscopicity which is common to both samples. Above 3 μm the spectra become fully saturated and featureless likely due to the presence of moisture.

Ammonium nitrate NH_4NO_3 reflectance spectra are reported in Figure 3e down to 70K. This NH_4^+ compound showed clear ammonium bands located at ~1.05, ~1.3, ~1.56, ~2.02 and ~2.2 μm. NO_3^- fundamental absorption bands were near 9.5 μm (ν_1, IR inactive), 12.0 μm (ν_2), 7.2 μm (ν_3) and 13.9 μm (ν_4) (Wu et al., 2007). Some N-O overtone and combination bands are probably present in the 2.5-7 μm range but were difficult to recognize due to the overlaps with NH_4^+-associated bands (Cloutis et al., 2016). In the spectral range above 3 μm NH_4^+ signals were evident at 3.02, 3.21, 3.40 and 3.49 μm. Absorption bands in the 4-5 μm range were assigned to NO_3^- overtones and combinations (Wu et al., 2007).

Solid NH_4NO_3 has four crystalline phase transitions corresponding to as many stable polymorphs (V ↔ IV ↔ III ↔ II ↔ I) in the temperature range from 130 to 443 K, this latter is the melting *T* (Fernandes et al., 1979; Theoret and Sandorfy, 1964). We observed the low *T* transformation (V ↔ IV at 256 K) to mainly affect the ν_1 and ν_4 bands of NH_4^+ and the ν_3 and ν_4 bands of NO_3^-, splitting them in several components (Fernandes et al., 1979). No spectral evidence of other phase transitions was detected in our data.

Ammonium phosphate $(NH_4)H_2PO_4$ reflectance spectra, at low *T*, were collected only up to 3.5 μm (Fig. 3g). The spectra of this mineral showed typical NH_4^+ absorption bands at ~1.07, 1.28, 1.58, and 2.2 μm. The PO_4^{3-} group has four normal modes (ν_1, ν_2, ν_3, ν_4) of which only the ν_3 stretching modes and ν_4 bending modes are infrared active and located at ~9 μm and ~ 19 μm, respectively (Stefov et al., 2004). Overtone and combination bands due to PO_4^{3-} can be detected in the 4-5 μm range (Berg et al., 2016). The NH_4^+ spectral features are identified as expected and their positions are consistent with those of the other ammonium-bearing minerals studied in this work. $(NH_4)H_2PO_4$ is a phosphate characterized by a low-*T* transition to a ferroelectric phase at ~153 K with a rearrangement of hydrogen bonds (Tenzer et al., 1958). Simon, (1989) analyzing the phonon spectra by infrared

reflectivity of ammonium phosphate in the para- and ferroelectric phases, found that the phase transition mainly affected the low-frequency modes, which disappear below T_c, and slightly impact on the NH_4^+ modes.

3.3 Effect of granulometry

The three different granulometries (125-150 µm: green spectra; 80-125 µm: red spectra; 32-80 µm: black spectra) affected the band parameters area, depth, and FWHM of the room *T* spectra. The band area, depth, FWHM and position evolutions for the analyzed bands are reported in Tab. 3. In general, the higher values of the area, depth and FWHM are found for the coarse (125-150 µm) and intermediate grain sizes (80-125 µm) and the band parameter evolutions were not always linear. In some cases, granulometry also affected band positions. We only considered shifts in the bands larger than 0.01 µm. For 1.06, 1.28, and 1.58 µm bands in mascagnite, the area and depth increase for larger grain sizes while the band at 2.13 µm had the opposite trend showing high values for the finest grain size (32-80 µm) (Fig. 2b). Salammoniac spectra exhibit high band area and depth values of the 1.08 1.31, 1.62 µm bands for the intermediate grain size, with a shift toward shorter wavelength of the 1.09 µm band for increasing grain size. The 2.2 µm band had the same behavior as that in the mascagnite spectra (Fig. 2d). For the hydrated sample larderellite high depth and area values are measured for the bands at 1.08, 1.32, and 2.10 µm in the intermediate granulometry spectrum (Fig. 2f). In struvite mineral, bands centered at 1.06 and 1.65 µm showed the maximum depth and area for the smallest and intermediate grain sizes, respectively. For the bands at 1.29 and 2.10 µm, their band depth assumed the maximum value for the coarse and fine grain size, respectively (Fig. 2h). Tschermigite spectra displayed a linear trend with granulometry for the 1.10, 1.22, 1.51, and 2.05 µm band depth and area parameters with the maximum for the coarse grain size (Fig. 2l). For the synthetic sample ammonium carbonate, the highest value of area and depth are found for the 1.09 and 1.28 µm bands for the medium grain size whereas for the bands at 1.64 and 2.12 µm the maximum is obtained for the coarse and fine grain sizes, respectively (Fig. 3b). In ammonium bicarbonate spectra the bands located at 1.09, 1.30, 1.62, and 2.14 µm have area and depth increasing linearly with granulometry. Ammonium nitrate displays the same spectral evolution of the band parameters with granulometry, except for the 2.12 µm mode displaying the highest values for the intermediate grain size (Fig. 3d). Lastly, ammonium phosphate has also the same spectral trend as the last two samples with a linear increase of band parameters with increasing grain size (Fig. 3f). In this case too, the band near ~2.10 µm has the highest parameter values for medium granulometry.

Table 3: Analyzed band parameters and their dependance with granulometry (G) for the samples studied in this work. Band assignments are reported in Table 2. The up/down arrows indicate the direction of change of the parameter for increasing granulometry. The left arrow indicates a shift towards shorter wavelengths while a right arrow indicates a shift towards longer wavelengths. The letter next to the arrow indicates which grain size corresponds to the highest value (f= fine 32-80 µm; m= medium 80-125 µm; c= coarse 125-150 µm).

Sample	Band (µm)	Position	FWHM	Depth	Area
Mascagnite	1.06	-	↓f	↑c	↑c
	1.28	-	↑c	↑c	↑c
	1.58	-	↑c	↑c	↑c
	2.13	-	↓f	↓f	↓f
Salammoniac	1.09	←	↑m	↑m	↑m
	1.32	-	↑c	↑m	↑m
	1.62	-	↑c	↑m	↑m
	2.14	-	↑m	↓f	↓f
Larderellite	1.05	→	↑c	-	↑c
	1.28	→	↑m	↑m	↑m
	1.54	-	↑c	↑c	↑m
	2.10	-	↑c	↑c	↓m

Struvite	1.06	-	↓f	-	-
	1.29	-	-	-	-
	1.65	-	↑c	↑c	↑c
	2.10	-	↓f	↓f	↓f
Tschermigite	1.10	-	↑c	-	↑c
	1.22	-	↑c	↑c	↑c
	1.51	-	↓f	↑c	↑c
	2.05	-	↓f	↑c	↑c
Ammonium carbonate	1.09	←	↑c	↑m	↑m
	1.28	→	↑m	↑m	↑m
	1.64	-	↑c	↑c	↑c
	2.12	-	↑c	↓f	-
Ammonium phosphate	1.07	-	↑m	↑c	↑c
	1.28	-	↑m	↑c	↑c
	1.58	-	↑m	↑c	↑c
	2.10	←	↑c	↑m	↑c
Ammonium nitrate	1.07	-	↑c	↑c	↑c
	1.28	-	↓f	↑c	↑c
	1.57	-	↑c	↑c	↑c
	2.12	-	↑c	↑m	↑m
Ammonium bicarbonate	1.09	←	↑c	↑c	↑c
	1.30	-	↑m	↑c	↑c
	1.62	-	↑c	↑c	↑m
	2.14	-	↑c	↑m	↑m

3.4 Effect of temperature

The effects of decreasing *T* on band parameters are reported in Fig. 4; 5; 6; 7, 8 and in Table 4. We focus on the low *T* behaviour of the ~1.06, 1.30, 1.56, 2.02 and 2.2 µm spectral features as characteristic of NH_4-bearing natural and synthetic compounds. We assessed their sensitivity to temperature variations and phase transition, with the exception of the tschermigite sample due to its high-water content and the resulting overlap of vibrational bands of NH_4^+ and H_2O.

Almost all band positions shifted toward higher wavelengths for decreasing temperature (a panel in Fig. 4; 5; 6; 7, 8). These shifts were strictly related to the increase of hydrogen bond strength as the *T* decreases. Both depth and area of the bands increased when the temperature decreased (b and c panels in Fig. 4; 5; 6; 7, 8). The bandwidth did not display a unique behavior as suggested by other authors (e.g., De Angelis et al., 2019), especially for the 1.06 µm bands (Fig. 5b and Table 4). The general deepening and increasing in the number of bands as temperature decreases was consistent with the narrowing of the absorption bands, which increased their definition and reduced the overlap with other spectral features. Both depth and area of the bands of compounds that undergo a low *T* phase transition showed a sudden change in values (e.g., Fig. 6b-c mascagnite, black square, after 223K or salammoniac, red circles, after 242K) and a linear evolution (see Tab. 4) at the T_c.

Spectral parameters for the 1.06 µm bands are reported in Fig. 4. This band likely resulted from the NH_4^+ $3\nu_3$ overtone mode. Its depth and area tended to increase with decreasing *T*, although the data showed nonlinear behaviors and even a reverse behavior for ammonium nitrate (green triangles in Fig. 4) and mascagnite (black squares in Fig. 4). Its band position moved to longer wavelengths. For the samples mascagnite (black squares Fig. 4), salammoniac (red circles Fig. 4), and ammonium

phosphate (cyan triangles Fig. 4) a change in band parameters can be seen at their transition temperature and also at approximately 150 K for salammoniac and mascagnite.

The spectral indices calculated for the 1.30 μm bands are reported in Fig. 5. This absorption band, due to the $2\nu_3 + \nu_4$ combination mode of the NH_4^+ groups showed a more linear behavior of the band parameters, compared to the previous one, in relation to temperature variation. The band position (Fig. 5a) slightly shifted towards higher wavelengths as the temperature decreased, excepted for ammonium phosphate below the phase T_c ~150K (cyan triangles in Fig. 5c). The band depth increased almost linearly at low *T* except for the samples mascagnite (black squares in Fig. 5c), ammonium carbonate (light brown triangles in Fig. 5c), ammonium bicarbonate (purple diamonds in Fig. 5c), and struvite (brown circles Fig. 5c) which have no clear trends. The first three samples had also no clear variation in band area; whereas salammoniac, mascagnite, and larderellite have increasing values at low *T*, and ammonium nitrate has the reverse trend.

In Fig. 6 we show the temperature behavior of the 1.56 μm band parameters. The band position shifts towards higher wavelengths with decreasing *T*, except for the salammoniac sample which showed an opposite trend (red circles in Fig. 6a). Both the depth and the area (Fig. 6 b-c) of the bands increased, except for samples undergoing a phase transition which showed a slow growth after an abrupt drop.

The 2.12 μm band was characterized by a doublet, with two separate minima occurring at ~2.02 and 2.2 μm. The parameters of these bands are shown in Fig.s 7 and 8, respectively. The band position for the 2.02 μm band (Fig. 7a) seemed to be almost not affected by temperature, whereas the position of the 2.2 μm band showed some slight shift towards shorter wavelengths for decreasing *T*, except for salammoniac which shifted in the reverse direction. Ammonia phosphate displayed a clear and sudden shift at a lower wavelength during its phase transition around 148 K, whereas mascagnite moved only slightly to a higher wavelength below 223 K. Both bands have their depth and area increasing with the reduction in temperature for all samples. These two absorption bands in salammoniac and mascagnite seemed to be less sensitive to phase transition than the previous ones, especially for the band position parameter. Both depth and area of the 2.12 μm band of ammonium phosphate display a drop at the phase transition, whereas, for the 2.02 μm spectral feature, only the band area is affected by the phase transition. The FWHM trends of the same absorption bands were quite variable in the different ammonium minerals with generally clear changes at the phase transition that, however, can be opposite for the two bands (Fig. s. 7d and 8d).

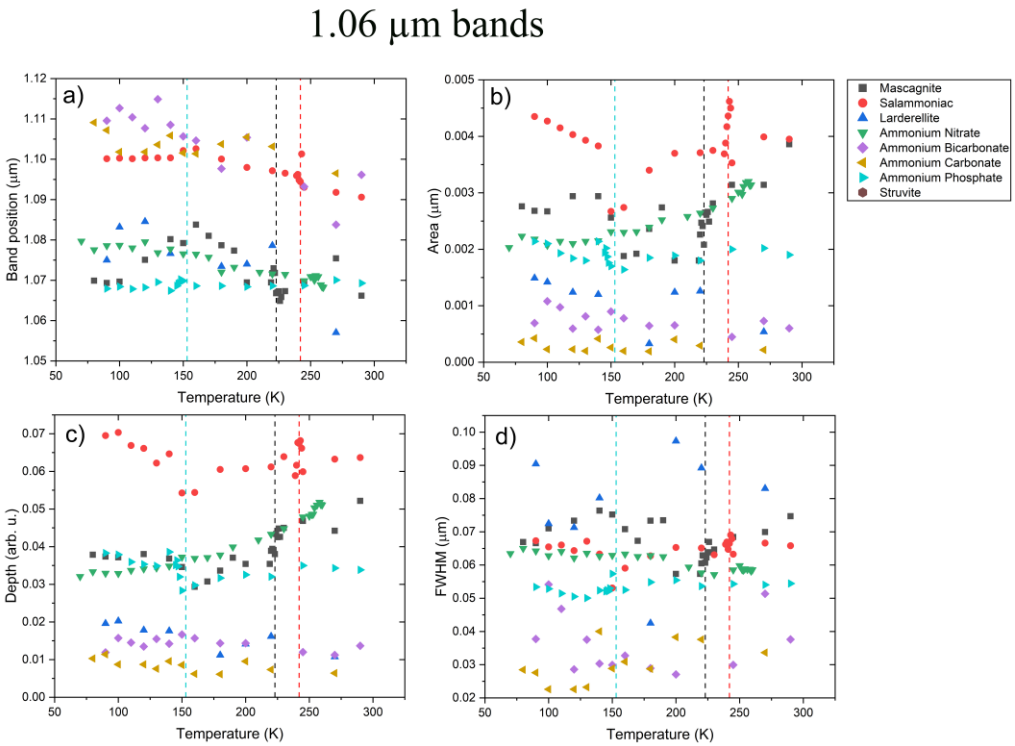

Fig.4: Band parameters of the 1.06 µm band for all samples with 32-80 µm grain size. a) band position in µm; b) area in µm; c) depth in arbitrary unit and d) full FWHM in µm. The dashed lines indicate the transition temperatures of minerals of the same color in the figures.

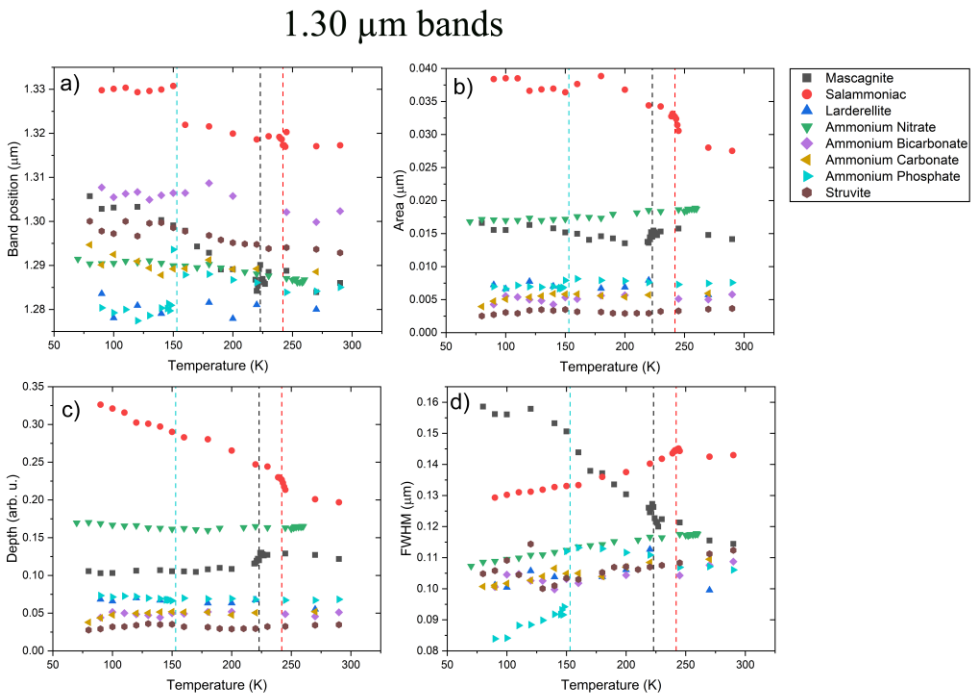

Fig.5: Band parameters of the 1.30 µm bands for all samples with 32-80 µm grain size. a) band position in µm; b) area in µm; c) depth in arbitrary unit and d) FWHM in µm. The dashed lines indicate the transition temperatures of minerals of the same color in the figures.

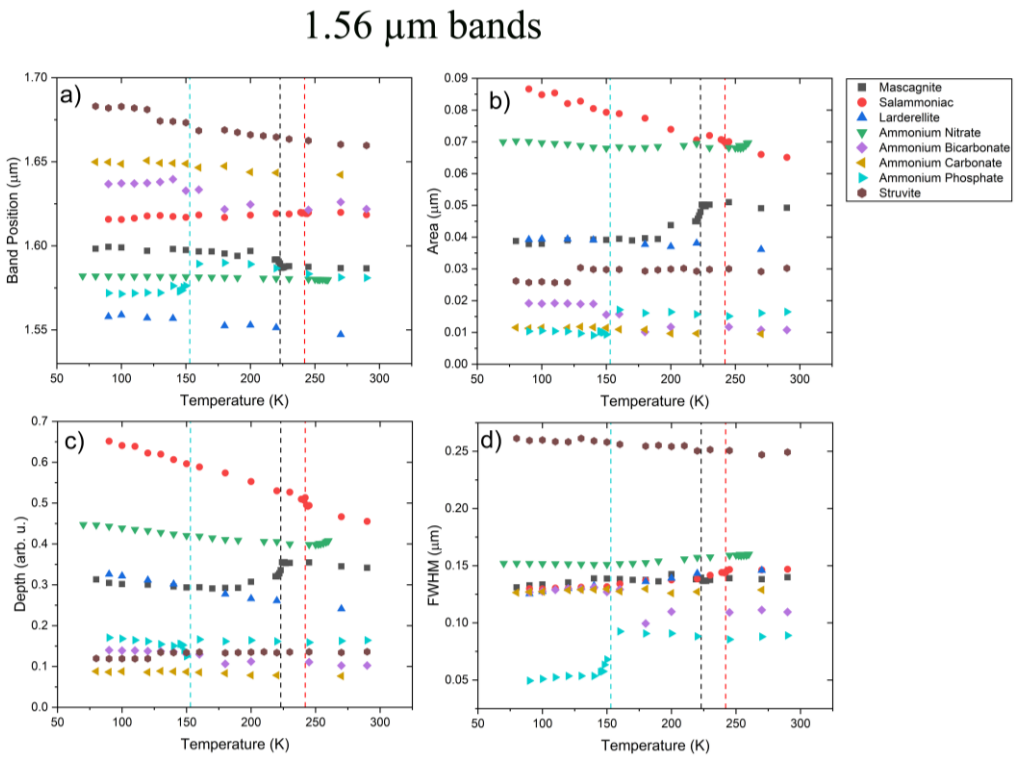

Fig.6: Band parameters of the 1.56 µm complex for all samples with 32-80 µm grain size. a) band position in µm; b) area in µm; c) depth in arbitrary unit and d) FWHM in µm. The dashed lines indicate the transition temperatures of minerals of the same color in the figures.

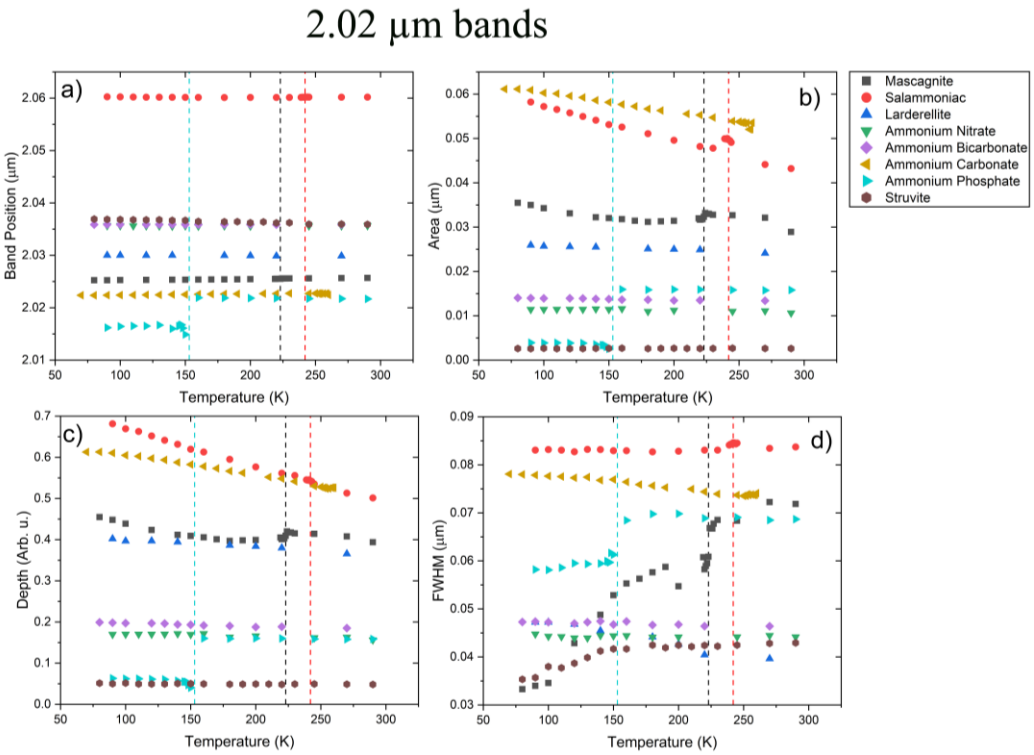

Fig.7: Band parameters of the 2.02 µm bands for all samples with 32-80 µm grain size. a) band position in µm; b) area in µm; c) depth in arbitrary unit and d) FWHM in µm. The dashed lines indicate the transition temperatures of minerals of the same color in the figures.

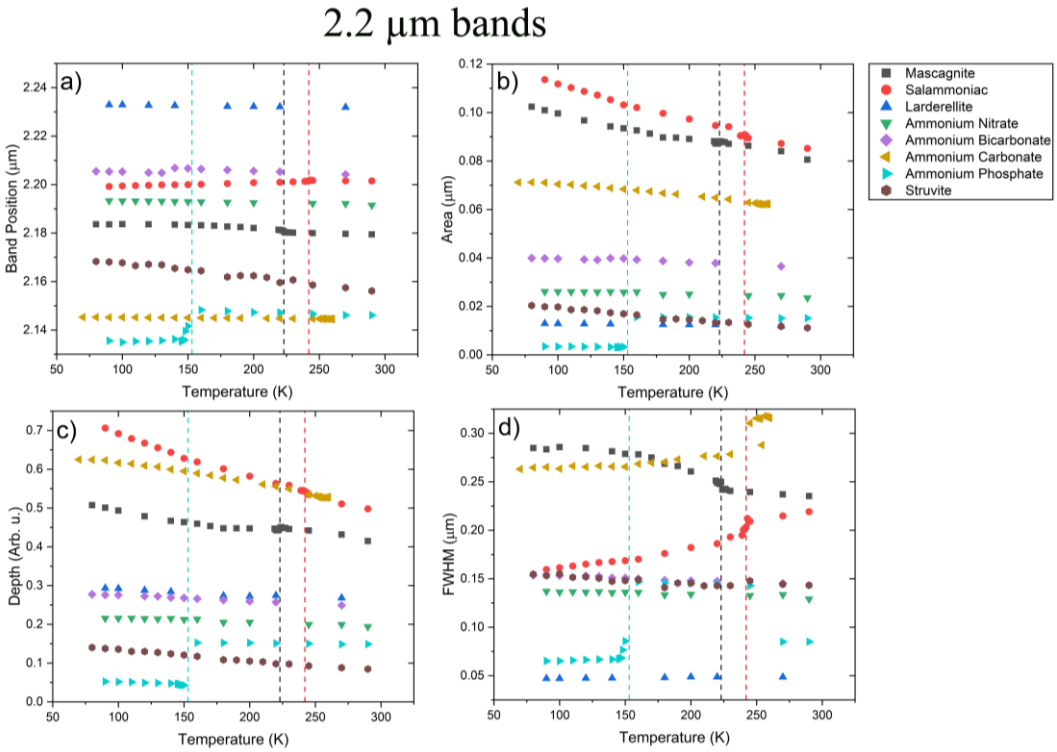

Fig.8: Band parameters of the 2.2 µm bands for all samples with 32-80 µm grain size. a) band position in µm; b) area in µm; c) depth in arbitrary unit and d) FWHM in µm. The dashed lines indicate the transition temperatures of minerals of the same color in the figures

Table 4: Analyzed band parameters and their dependence on temperature (*T*) for the samples studied in this work. Band assignments are reported in Table 2. The Band positions (B_p) Δ B_p /T, Δ area/T, Δ depth/T and Δ FWH/T, namely the sensitivity of these parameters with *T*, are reported. The positions of the bands are taken at room *T*. These global values are obtained from a linear fit with a single line considering all points within the graphs for samples not affected by phase transitions. For samples affected by phase transitions, two fit values before and after the transition *T* were reported. The values between the square brackets indicate R^2 of the fit.

Samples	**B_p (µm)**	**Δ B_p/T * 10^{-5} (µm.K^{-1})**	**Δ FWHM/T * 10^{-5} (µm.K^{-1})**	**Δ depth/T * 10^{-5} (K^{-1})**	**Δ area/T * 10^{-5} (µm.K^{-1})**
Mascagnite	1.06	-; 6.4 [0.24]	-	9.0 [0.44]; -3.6 [0.24]	1.5 [0.82]; 0.6 [0.43]
$(NH_4)_2SO_4$	1.28	- 6.28 [0.53]; -14.5 [0.93]	-14.0 [0.94]; -24 [0.87]	- 9.3 [0.61]; 5.0 [0.60]	- 2.3 [0.76]; -2.0 [0.82]
	1.58	-2.2 [0.94]; -3.7 [0.70]	2.75 [0.53]; 5.6 [0.64]	-23.0 [0.90]; -16.0 [0.80]	-2.5 [0.57]; 1.2 [0.61]
	2.02	0.2 [0.98]; 1.6 [0.98]	7.0 [0.79]; 23.0 [0.91]	-34.9 [0.88]; 50.0 [0.93]	-6 [0.75]; -3.6 [0.92]
	2.18	-1.2 [0.99]; -1.2 [0.80]	9.0 [0.99];-19.0 [0.81]	-51.0 [0.94]; -53 [0.97]	-10.0 [0.67]; - 15.0 [0.86]
Salammoniac	1.09	-5.5 [0.99]; 7.8 [0.95]; 0.4 [0.60]	-	8.5 [0.87]; 11.0 [0.86]; -14 [0.76]	0.9 [0.73]; 1.3 [0.80]; -1.0 [0.99]
NH_4Cl	1.32	0.7 [0.96]; -9 [0.85]	-4.5 [0.68]; 8.5 [0.96]	-43.0 [0.93]; -57 [0.98]	-8.2 [0.90]; -2.32 [0.51]
	1.62	1.9 [0.75]	0.8 [0.63]; 7.8 [0.90]	-86.0 [98]; -92.0 [0.99]	-9.7 [0.88]; - 11.0 [0.97]
	2.06	-	-	-76.0 [0.99]; -93.0 [0.99]	-13.0 [0.90]; 7.5 [0.99]
	2.20	-0.5 [0.98]; 1.3 [0.99]	21.0 [0.99]; 20.0 [0.97]	-84.0 [0.99]; -106.0 [0.99]	-34.0 [0.96]; 30.0 [0.98]
Larderellite	1.05	-9.8 [0.54]	-	-4.81 [0.71]	-0.4 [0.38]
$(NH_4)B_5O_7(OH)_2 \cdot H_2O$	1.28	-	-	-5.6 [0.57]	-
	1.55	-6.2 [0.96]	11.6 [0.98]	-49.0 [0.99]	-1.81 [0.85]
	2.03	-	-4.7 [0.96]	-18.4 [0.96]	-0.9 [0.96]
	2.23	-	1.0 [0.83]	-14.9 [0.92]	-0.5 [0.95]

Struvite	-	-	-	-	-
$(NH_4)MgPO_4 \cdot 6H_2O$	1.29	-3.3 [0.78]	2.5 [0.17]	-	-
	1.65	-12.7 [0.93]	-6.5 [0.90]	8.8 [0.76]	2.06 [0.50]
	2.04	-0.5 [0.95]	3.4 [0.74]	-1.0 [0.55]	-
	2.15	-6.0 [0.97]	-5.8 [0.67]	-0.3 [0.99]	-4.62 [0.98]
Ammonium carbonate	1.09	-3.6 [0.39]	6.3 [0.34]	-1.9 [0.41]	-
$(NH_4)_2CO_3$	1.28	-2.0 [0.35]	4.8 [0.86]	4.5 [0.37]	0.7 [0.46]
	1.64	-4.6 [0.84]	24.0 [0.95]	-6.9 [0.81]	-1.3 [0.76]
	2.03	-	-0.5 [0.65]	-7.9 [0.96]	-0.4 [0.92]
	2.20	-	-4.9 [0.96]	-15.2 [0.99]	-1.7 [0.85]
Ammonium phosphate	1.07	0.5 [0.61]; 1.5 [0.20]	-	3.2 [0.73]; - 9.3 [0.92]	-
$(NH_4)H_2PO_4$	1.28	3.1 [0.70]; -	-6.0 [0.92]; 16.0 [0.93]	-2.65 [0.77]	-0.1 [0.98]; - 0.4 [0.36]
	1.58	-9.14 [0.96]; 1.57 [0.34]	-3.4 [0.48]; 8.5 [0.84]	- ; -41.0 [0.97]	-1.14 [0.50]; -2.6 [0.72]
	2.02	0.2 [0.98]; -	-22.0 [0.34]; 2.6 [0.53]	-1.57 [0.69]; -9.9 [0.80]	- 0.1 [0.63]; -0.8 [0.70]
	2.15	-1.72 [0.98];	-; 4.0 [0.92]	- 3.4 [0.94]; -9.5 [0.98]	-0.3 [0.77]; -0.5 [0.94]
Ammonium nitrate	1.07	-5.6 [0.92]	-3.4 [0.82]	10.5 [0.93]	0.6 [0.89]
NH_4NO_3	1.28	-2.7 [0.89]	5.1 [0.98]	-1.9 [0.23]	1.06 [0.91]
	1.57	-1.3 [0.97]	5.0 [0.84]	-23.9 [0.95]	-0.6 [0.26]
	2.02	0.2 [0.74]	-2.6 [0.97]	-50.6 [0.99]	-4.53 [0.98]
	2.14	-0.4 [0.98]; 1.5 [0.5]	29.2 [0.74]	-56.5 [0.98]	-5.22 [0.99]
Ammonium bicarbonate	1.09	-11.7 [0.76]	-	-1.1 [0.18]	-
$(NH_4)HCO_3$	1.30	-2.8 [0.57]	2.8 [0.53]	-	0.3 [0.16]
	1.62	-9.3 [0.73]	-12.6 [0.56]	-21.9 [0.87]	-5.2 [0.78]

	2.03 2.19	- -0.8 [0.95]	- -3.1 [0.82]	-6.5 [0.79] -11.2 [0.94]	-0.3 [0.68] -1.2 [0.89]

6

4 Discussion

Numerous absorption bands were identified in the VIS-NIR spectra of the natural and synthetic ammonium-bearing compounds presented in this works (Table 2). The main bands are due to overtones and combinations of NH_4^+ groups and they are present in the spectra of both natural and synthetic samples (Fig.2 and 3) especially at ~1.07, 1.28, 1.58, and 2.12 µm (Krohn and Altaner, 1987). A band representing the fundamental mode of NH_4^+ asymmetric stretch is observed at ~3.03 µm (Harlov et al., 2001 a, b, c; Bishop et al., 2002). In the ammonium carbonate and ammonium bicarbonate spectra, many similarities are observed. Most notable are the bands located below the 3 µm spectral range and the absence of CO_3^{2-} vibrational modes. Probably these affinities can be attributed to the high hygroscopicity of ammonium carbonate samples. Water spectral features are generally strong and tend to overlap the ammonium ones. The strong intensity of the H_2O bands is the reason for the overall attenuation of the NH_4^+ absorption bands in hydrated samples also in nominally anhydrous samples.

Larderellite, struvite, and tschermigite ammonium minerals are characterized by an increase in structural water amount from 15 wt % in larderellite to 48 wt % in tschermigite. These series of hydrated minerals display a reduction in the number and definition of bands in relation to their water content (Fig. 1 left). H_2O has strong fundamental absorption bands at ~2.9 µm (Clark et al., 1990) and in the 3-3.7 µm range; NH_4^+ also generates strong absorption bands (Berg et al., 2016). Hydrated samples evidently show how ammonium peaks are progressively obscured as the water content increases. In addition, the differences in band position in the 3-3.7 µm range can be also affected by the presence of H_2O (Max and Chapados, 2013). Moreover, together with water increase, these samples show a shift toward shorter wavelength of the 3 µm bands with an overall reflectance intensity decrease and an increase in the NIR slope in the first part of the spectra (Fig. 1). For the above-mentioned reasons, the detection and assignment of characteristic NH_4^+ absorption bands become complicated in hydrated compounds.

The spectral differences between minerals (e.g., salammoniac and mascagnite, Fig.1), especially in the definition and number of absorption bands, might be attributed to the reduction in symmetry of the NH_4^+ group in the crystal structure (Felzer, 1990) that mainly affects the bands located at ~1.08 and ~1.3 µm (Berg et al., 2016). The bands at ~1.56, 2.02, and 2.2 µm are present in both natural and synthetic samples. Moreover, bands positions can be affected by different strengths of the hydrogen bonds (Cloutis et al., 2006) that consequently affect the distance between donor-acceptor in the crystal structure (Comodi et al., 2021).

4.1 Phase transitions in NH_4^+-bearing minerals

The ammonium ion is well known because of its propensity to reorient and give rise to several crystal structure (Moriya et al., 1977) with subsequent rearrangement at low temperature. In fact, the tetrahedral ammonium ion can generate favourable hydrogen bonding in the tetrahedral symmetry site (Smith, 1994). In the solid-state, NH_4^+ ion may have several equivalent orientations and if two or more of these positions occur in the same crystal site, the structure can become disordered (Smith, 1994). In addition, para- to ferroelectric phase transitions mainly affect hydrogen bonds, which are strengthened in the case of the mascagnite sample (Schlemper and Hamilton, 1966). For this reason, in the low-*T* spectra of tschermigite and ammonium nitrate, we did not identify any spectral variation due to phase transitions. In the examined spectral range, we can evaluate the effect of the

transformations that affect either the NH_4^+ ion or the hydrogen bonds as they generate additional absorption bands in the spectra of the selected ammonium minerals.

Abdeen et al. (1981) report that the disordered sulfate tetrahedra in $(NH_4)Al(SO_4)_2 \cdot 12H_2O$ structure are distorted and in a reversed orientation. Recently, Mhiri (2011) confirmed the hypothesis of a disordered orientation for sulfate groups in the tschermigite structure. For these reasons the phase transition in this mineral mainly affects the SO_4 tetrahedra. To our knowledge, no detailed information on the low-*T* behavior of this mineral is given in literature.

Ammonium nitrate is characterized by a low-temperature phase transition from the V → IV structures that consist in a change in space group and symmetry, but the crystal ordering remains stable, the NH_4^+ ion does not rotate at low *T* and the bond strength between the atoms remain strong (Ahtee et al., 1983), consequently no spectral change was observed.

In mascagnite $(NH_4)_2SO_4$ a transformation occurs below 223K, the structure becoming ferroelectric (Schlemper and Hamilton, 1966; Schutte and Heyns, 1970). As reported by Schlemper and Hamilton (1966), in the ferroelectric phase the distortion of ammonium ions I and II is less than paraelectric state, the sulfate tetrahedra are not strongly distorted and their geometry does not vary considerably between the two phases (Schutte and Heyns, 1970). Ammonium sulfate spectra (Fig. 2a), below the phase transition *T*, show changes in intensities of combination and overtone bands (Fig. 5c, 6c, 7c, 8c). These variations can be ascribed to a strengthening of hydrogen bonds (Bratož and Hadži, 1957) following data from Schlemper and Hamilton (1966) and Schutte and Heyns (1970). Due to the nature of the transition, we do not have large spectral variations, as for salammoniac and ammonium phosphate. The most obvious changes of the mascagnite spectrum below the T_c are at 1.8 μm with the growth of a new band and the change of spectrum slope at ~ 2.6 μm, where several weak bands also emerge (Fig. 9).

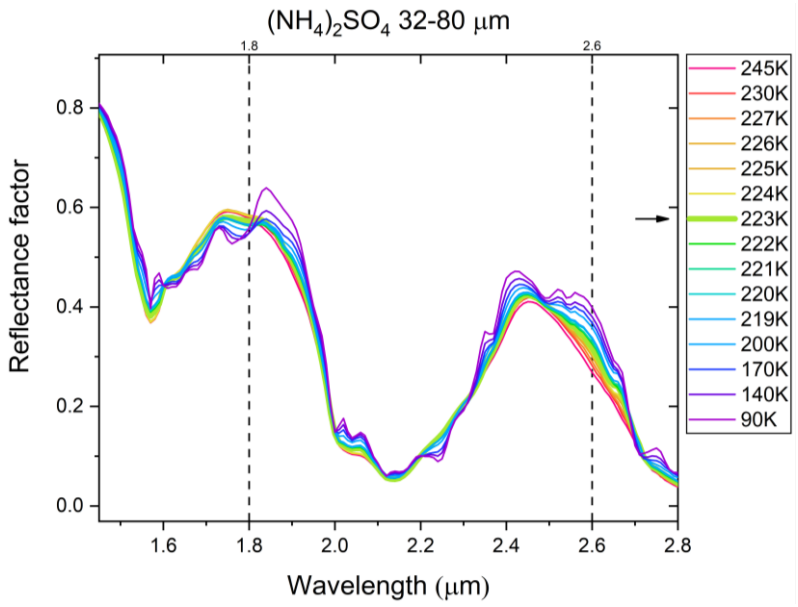

Fig.9: Reflectance spectra of mascagnite at low temperature in the 1.45-2.8 μm spectral range. Its phase transition occurs at 223 K (underling by arrow). The main changes during phase transition are the growth of a band at 1.8 μm and changes in the spectral range around 2.6 μm, highlighted by dashed black lines.

Reflectance spectra of salammoniac NH_4Cl (Fig. 2c) shows the effect of the ordering of hydrogen bonds. Below 242 K an order-disorder phase transition (λ-transition) occurs. In the spectral region above 2.5 μm, corresponding to the fundamental stretching region, combination and overtone bands of the NH_4^+ group were observed below the transition *T*. At room temperature, hydrogen bonding in the same spectral region, generates broad bands due to the complex vibrational modes of NH_4^+ ion in relation to the wide range of positions, distances and orientations. The evidence of the formation of hydrogen bonds is the downward shift of the NH_4^+ stretching frequencies (e.g., $2\nu_3$) and the upward shift of bending mode frequencies (Waddington, 1958). Bands located at ~ 2.62 ($\nu_3 + 2\nu_6$), 2.83 ($\nu_3 + \nu_6$), 3.24 ($\nu_2+\nu_4$) and 3.72 μm ($\nu_2 + 2\nu_6$) show the largest temperature dependence of both position and intensity, as shown in Fig. 11b (black dashed lines) and their shift towards low wavelength (solid black lines in Fig. 11b). In addition, the bands, grown to ~1.80, 2.74 ($\nu_3 + \nu_6$), 2.91 ($\nu_1 + \nu_{5TO}$) and 4.06 ($\nu_4 + \nu_6 + \nu_{5LO}$) μm, with the assignations made following Schumaker and Garland, 1970, are a further confirmation of the occurring phase transition (red dash lines in Fig. 10a, b).

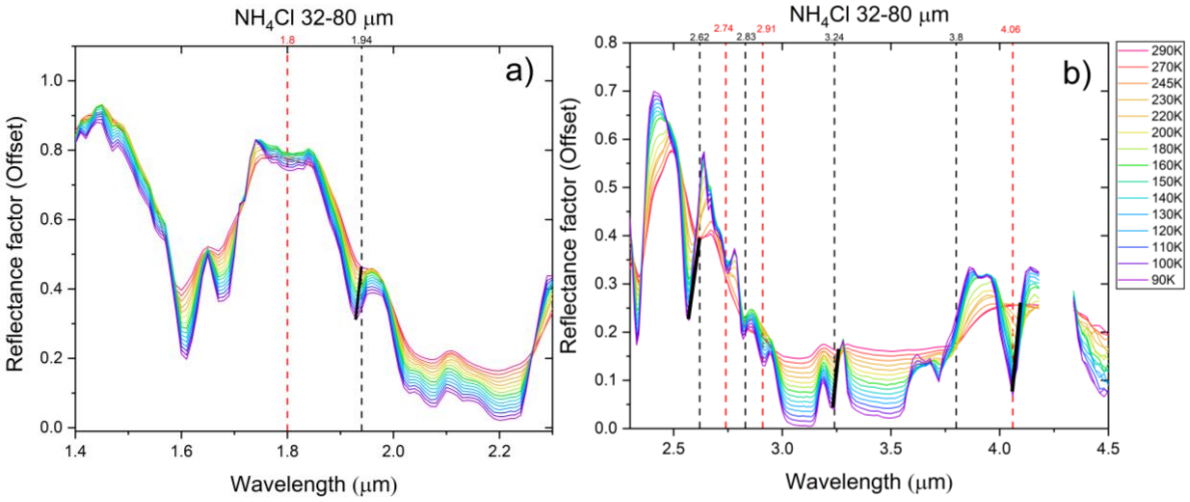

Fig.10: Reflectance spectra of ammonium chloride (a) in the 1.4-2.3 μm spectral range to highlight the band growth at 1.8 μm below 230K, and (b) in the 2.3-4.5μm spectral range to highlight the shift and appearance of new bands at ~ 2.62, 2.74, 2.83, 2.9, 3.24, 3.72 and 4.06 μm (b). Red dash lines indicate new bands appearing below the phase transition, while black dash lines indicate bands with large shifts towards low wavelength at low temperature. The spectra have been offset vertically for clarity

The effect of low *T* on the behavior 2.62 ($3\nu_4$), 2.83 ($2\nu_2$), 3.24 ($\nu_2 + \nu_4$) and 3.72 ($2\nu_4$) μm bands can be excluded. Looking in detail at the absorption band at 2.6 (Fig. 11) μm in the temperature range around the phase transition, it is possible to notice the clear shift in wavelengths (approximately 0.015), an effect due to the phase transition and not to the low *T*.

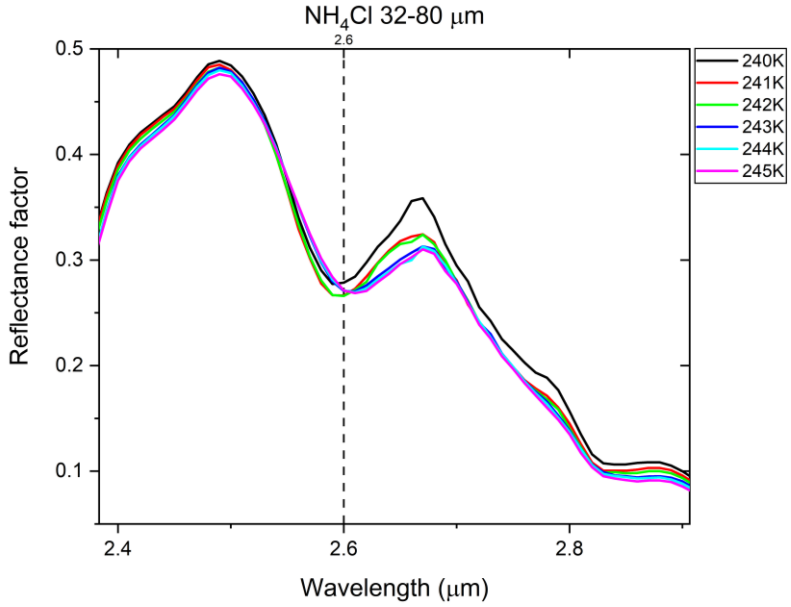

Fig. 11: Reflectance spectra of ammonium chloride in the 2.4-2.9 µm spectral range to evaluate the band shift at ~2.6 µm in the 240-245 K *T* range highlighted by the black dash line.

Ammonium phosphate undergoes a para- to an antiferroelectric phase transition, with an order-disorder mechanism at 148 K (Fukai et al., 1987). In the structure of ammonium phosphate, two kinds of hydrogen bonds link NH_4^+ and PO_4^{3-} ions: O-H···O and N-H···O. The coupling between these two types of hydrogen bonds generates the antiferroelectric behavior with the possibility of forming extra hydrogen bonds between N and O (Matsushita and Matsubara, 1986). Also, for this synthetic ammonium salt, the phase transition was detected by the overtone and combination bands of the NH_4^+ groups as it affects hydrogen bonds. The vibrational modes at ~ 1.03, 1.30, 1.56, 2.02, and 2.2 µm are sensitive to this transformation with an abrupt change in the band parameters below 148 K (Fig. 5, 6, 7, 8 cyan triangles). The spectral details shown in Fig. 12 emphasizes the effect of phase transition in the spectra below ~150K (green curves).

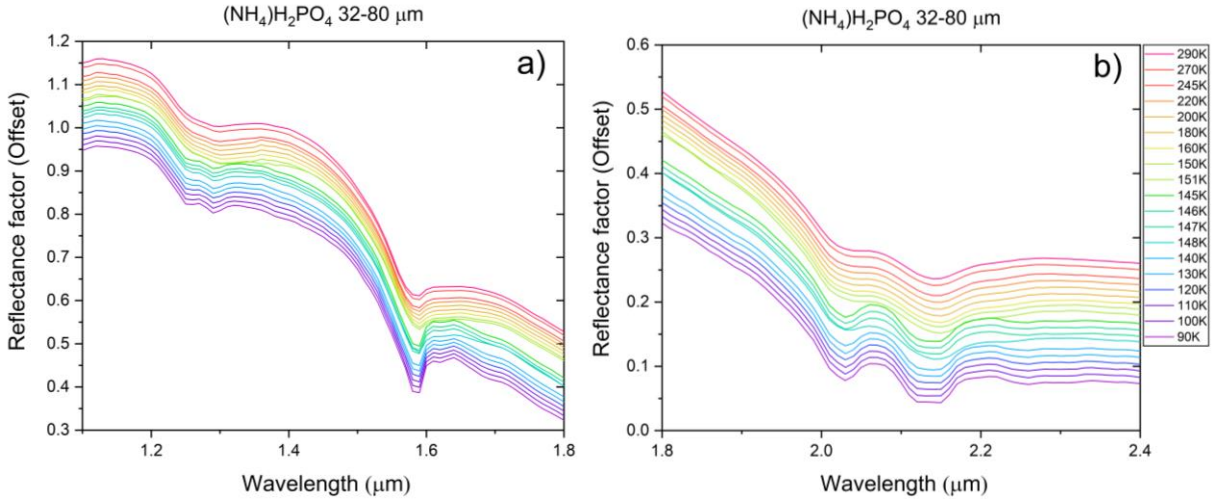

Fig.12: Reflectance spectra of ammonium phosphate in (a) the 1.1-1.8 µm and (b) the 1.8-2.4 µm spectral ranges to highlight the band changes below ~150K (green spectra). The spectra have been offset vertically for clear

4.2 Applications to icy objects

Cook et al. (2007) found variations of the position of the band at 2.21 μm in the spectrum of Charon at different subsolar longitudes, suggesting the existence of various ammonia hydration states across its surface. Furthermore, Cook et al. (2018) modeled the spectra of Charon's surface using data for anhydrous NH_4^+ minerals, due to the lack of spectral data on these salts, especially the hydrated forms at low temperature. Pluto also shows ammonia bands at ~1.65 and 2.21 μm in the Virgil Fossae area (Dalle Ore et al., 2019), and these signatures can be attributed to ammonium-bearing minerals even if with some ambiguity due to the similarity of the absorption bands to H_2O ice (Cruikshank et al., 2019). NH_4^+ is extracted from the fluid by the production of minerals and salts (Cruikshank et al., 2019). If ammonia would be present in the form of minerals and salts, it would also be more resistant to destruction by space weathering (Cruikshank et al., 2019). Cook et al. (2018) also found that salammoniac (NH_4Cl) gives a good fit of the NH_4^+ band observed in both Nix and Hydra spectra recorded by *New Horizons*. Ammonium minerals, such as $(NH_4)_2SO_4$ and NH_4Cl can constitute a significant minor part of the low-*T* ammonia-rich solution. These minerals have dissolution rates and solubility different from one to another, influencing some physical properties. Their identification could have a strong impact on models that examine the relationship between the phases present within the presumed oceans and environments that are or have been present on Pluto and other icy bodies.

Concerning the Ceres' spectrum and the absorption features located at 2.21 μm, ascribed to the presence of NH_4^+ salts, the collected data can give some additional information. From the sample set analyzed, it emerges that the two samples salammoniac and ammonium bicarbonate have the best band position affinity at 2.21 μm under room *T* as proposed in De Sanctis et al., 2016. On the other hand, and as reported in this work, with decreasing *T* the 2.2 μm on NH_4Cl sample shifts toward shorter wavelength. At temperature hypothesized on Ceres' surface the salammoniac undergoes a phase transition, that changes the overall spectrum and should induce significant spectral modifications when it is added in some surface mixing models, which should allow to definitively clarify the presence or not of salammoniac and Ceres' surface.

Furthermore, the band located at ~3.05 μm is also related to the presence of ammonium compounds. In our spectra this band is well identified in mascagnite, salammoniac and ammonium nitrate minerals as a broad and water-saturated band, as reported by other authors (e.g., Ferrari et al., 2019; Ehlman et al., 2018). Even if their band position might be in good agreement with the features found on Ceres' spectra, their band parameters, namely depth and area and the shape are not similar.

In addition, to help to understand the composition of the Pluto system, these medium/high-resolution spectral data at low *T* can be helpful for the two future missions towards the Jovian icy satellites, NASA *Europa Clipper* and ESA *JUICE*. The two imaging spectrometers onboard these missions have the task to detect the non-water material on the surface of the Galilean moons, in particular Europa and Ganymede which appear to have a similar surface composition as shown by hyperspectral data from *Galileo* NIMS spectrometer (McCord et al., 1998). On the surface of these bodies, the presence of minerals has been presumed, including sulfates, carbonates, and chlorides (McCord et al., 1999; Ligier et al., 2016; Carlson et al., 2009; Comodi et al. 2014; Comodi et al., 2017). There is no evidence of NH_4^+ compounds on the surface, but in relation to the presence of subsurface oceans and the possibility of a fresh surface due to plumes/cryovolcanism activity (Sparks et al., 2016; Jia et al., 2018), the discovery of ammonium-bearing minerals could provide insights into the phenomena taking place in the interior of these bodies. Ammonia can form hydrogen bonds with water, thus

helping to stabilize various hydrate structures (Journaux et al., 2020). Moreover, these cryogenic data may be useful for the interpretations of forthcoming observations by the Near-Infrared Spectrograph (NIRSpec) (Rauscher et al., 2007) on board the James Webb Space Telescope (JWST) of Trans Neptunian Object (TNO).

In this scenario the use of laboratory data covering the same spectral range as the spacecraft instrument and at temperatures as close as possible to those of the surface of these bodies will strongly help to resolve some ambiguities in solid-phase determination. In particular, the hydrated NH_4^+ minerals, if present, should be in their low-*T* phases which have drastically different spectra and absorption band parameters than the room *T* phases, generally used, until now, to interpret icy satellites data. The consideration of the dependence of the spectra with temperature and particle size will be crucial for the spectral unmixing models of the hyperspectral data of the surface that will be recorded and thus for the correct identification of the mineral phases present at the surface. The spectral bands most affected by low *T* and phase transitions can be used as a temperature-dependent tool to hypothesize the surface conditions of the celestial bodies in which they are detected. Notably, spectra with clear phase transformations show substantial changes in band parameters and are therefore recognizable in their low *T* phase. Lastly, transitions can have a strong impact on internal dynamics such as convective flow on the crust as shown by Fortes and Choukroun (2010) for Titan's interior in relation to the presence of mascagnite.

5 Conclusions

In this work, we study the near infrared spectra at cryogenic temperature of a set of nine ammonium salts in three different grain sizes. We analyze the behavior of five bands characteristic of the NH_4^+ ion in relation to the low temperature. With cooling, their spectra show several common characteristics: (i) spectral features become more defined and the spectra show a more detailed structure; (ii) the band parameters, especially area and depth, generally increase with decreasing temperature and (iii) phase transitions, when detected, affect drastically the band positions due to the change of N-H···X hydrogen bond. Ammonium bearing minerals exhibit characteristic spectral features in the VIS and NIR ranges that should allow their detection on planetary bodies by remote sensing, if they are present. The useful absorption bands of ammonium salts are mostly below 2.5 μm. Characteristic NH_4^+ absorption bands are located at ~1.06, 1.3, 1.56 and 2.02 and 2.2 μm. Their band positions are related to the strength of the hydrogen bonds inside the crystal structure and they are very sensitive to the change of temperature and granulometry. In hydrated salts the number and definition of absorption bands are reduced with increasing water content. The water amount affects the position and shape of the 3 μm features, too. These laboratory spectra, adding information on the band dependences on composition, temperature and granulometry of some ammonium-bearing minerals, should aid the interpretation of remote data from the *New Horizons* LEISA spectrometer about Pluto's surface and its moons. The identification of ammonium minerals on the surface of planetary bodies will have a great impact because of the implications it will have on their internal composition.

On-line data

The complete sets of data (Fastelli et al., 2020a, b, c, d, e, f, g, h) presented in this paper are available online upon publication of this paper in the CSS database of the SSHADE database infrastructure (https://vwww.sshade.eu):

Fastelli, Maximiliano; Schmitt, Bernard; Beck, Pierre; Poch, Olivier (2020a): Near-infrared reflectance spectra at low temperature (300-90K) of Larderellite [(NH4)B5O7(OH)2.H2O] powders with three grain size ranges (32-80, 80-125 and 125-150µm). SSHADE/CSS (OSUG Data Center). Dataset/Spectral Data. doi:10.26302/SSHADE/EXPERIMENT_BS_20201114_009

Fastelli, Maximiliano; Schmitt, Bernard; Beck, Pierre; Poch, Olivier (2020b): Near-infrared reflectance spectra at low temperature (300-80K) of Struvite [(NH4)MgPO4·6(H2O)] powders with three grain size ranges (32-80, 80-125 and 125-150µm). SSHADE/CSS (OSUG Data Center). Dataset/Spectral Data. doi:10.26302/SSHADE/EXPERIMENT_BS_20201114_010

Fastelli, Maximiliano; Schmitt, Bernard; Beck, Pierre; Poch, Olivier (2020c): Near-infrared reflectance spectra at low temperature (300-90K) of Salammoniac and delta-Ammonium chloride (phase IV) [NH4Cl] powders with three grain size ranges (32-80, 80-125 and 125-150µm). SSHADE/CSS (OSUG Data Center). Dataset/Spectral Data. doi:10.26302/SSHADE/EXPERIMENT_BS_20201114_012

Fastelli, Maximiliano; Schmitt, Bernard; Beck, Pierre; Poch, Olivier (2020d): Near-infrared reflectance spectra at low temperature (300-90K) of Ammonium bicarbonate [(NH4)HCO3] powders with three grain size ranges (32-80, 80-125 and 125-150µm). SSHADE/CSS (OSUG Data Center). Dataset/Spectral Data. doi:10.26302/SSHADE/EXPERIMENT_BS_20201114_014

Fastelli, Maximiliano; Schmitt, Bernard; Beck, Pierre; Poch, Olivier (2020e): Near-infrared reflectance spectra at low temperature (300-70K) of Ammonium nitrate-IV and -V [(NH4)NO3] powders with three grain size ranges (32-80, 80-125 and 125-150µm). SSHADE/CSS (OSUG Data Center). Dataset/Spectral Data. doi:10.26302/SSHADE/EXPERIMENT_BS_20201114_015

Fastelli, Maximiliano; Schmitt, Bernard; Beck, Pierre; Poch, Olivier (2020f): Near-infrared reflectance spectra at low temperature (300-80K) of Ammonium carbonate [(NH4)2CO3] powders with three grain size ranges (32-80, 80-125 and 125-150µm). SSHADE/CSS (OSUG Data Center). Dataset/Spectral Data. doi:10.26302/SSHADE/EXPERIMENT_BS_20201114_016

Fastelli, Maximiliano; Schmitt, Bernard; Beck, Pierre; Poch, Olivier (2020g): Near-infrared reflectance spectra at low temperature (300-80K) of PE and AFE Ammonium biphosphate [(NH4)H2PO4] powders with three grain size ranges (32-80, 80-125 and 125-150µm). SSHADE/CSS (OSUG Data Center). Dataset/Spectral Data. doi:10.26302/SSHADE/EXPERIMENT_BS_20201114_017

Fastelli, Maximiliano; Schmitt, Bernard; Beck, Pierre; Poch, Olivier (2020h): Near-infrared reflectance spectra at low temperature (300-80K) of Mascagnite [(NH4)2SO4] powders with three grain size ranges (32-80, 80-125 and 125-150µm). SSHADE/CSS (OSUG Data Center). Dataset/Spectral Data. doi:10.26302/SSHADE/EXPERIMENT_BS_20201114_018

Acknowledgements

This work has been done in the frame of the Trans-National access program of Europlanet 2024 RI which has received funding from the European Union's Horizon 2020 research and innovation programme under grant agreement No 871149. PB acknowledges funding from the European Research Council (ERC) (SOLARYS ERC-CoG2017_771691)

Bibliography

- Ahtee, M., Smolander, K. J., Lucas, B. W., & Hewat, A. W. (1983). The structure of the low-temperature phase V of ammonium nitrate, ND_4NO_3. Acta Crystallographica Section C: Crystal Structure Communications, 39(6), 651-655.
- Balić-Žunić, T., Birkedal, R., Katerinopoulou, A., Comodi, P.; (2016) b. Dehydration of blödite, Na_2Mg (SO_4) $2(H_2O)_4$, and leonite, K_2Mg $(SO_4)_2$ (H_2O) 4. European Journal of Mineralogy, 28(1), 33-42.
- Balić-Žunić, T., Garavelli, A., Jakobsson, S. P., Jonasson, K., Katerinopoulos, A., Kyriakopoulos, K., & Acquafredda, P. (2016) a. Fumarolic minerals: An overview of active European volcanoes. Updates in Volcanology-From Volcano Modelling to Volcano Geology, 267-322.
- Berg, B. L., Cloutis, E. A., Beck, P., Vernazza, P., Bishop, J. L., Takir, D., Mann, P. (2016). Reflectance spectroscopy (0.35–8 μm) of ammonium-bearing minerals and qualitative comparison to Ceres-like asteroids. Icarus, 265, 218-237.
- Bishop, J. L., Banin, A., Mancinelli, R. L., Klovstad, M. R. (2002). Detection of soluble and fixed NH_4^+ in clay minerals by DTA and IR reflectance spectroscopy: a potential tool for planetary surface exploration. Planetary and Space Science, 50(1), 11-19.
- Bohmer, R., Lunkenheimer, P., Vij, J. K., Svare, I. (1990). Correlated reorientations in NH_4Al $(SO_4)_2.12H_2O$ single. Journal of Physics: Condensed Matter, 2(24), 5433.
- Bratož, S.; Hadži, D. (1957). Infrared spectra of molecules with hydrogen bonds. The Journal of Chemical Physics, 27(5), 991-997.
- Brissaud, O., Schmitt, B., Bonnefoy, N., Doute, S., Rabou, P., Grundy, W., Fily, M. (2004). Spectrogonio radiometer for the study of the bidirectional reflectance and polarization functions of planetary surfaces. 1. Design and tests. Applied Optics, 43(9), 1926-1937.
- Carlson, R.W., Calvin, W.M., Dalton, J.B., Hansen, G.B., Hudson, R.L., Johnson, R.E., McCord, T.B., Moore, M.H., 2009. Europa's Surface Composition, Europa. In: Pappalardo, R.T., McKinnon, W.B., Khurana, K.K. (Eds.), University of Arizona Press, Tucson, pp. 2009 with the assistance of René Dotson with 85 collaborating authorsThe University of Arizona space science series ISBN: 9780816528448, p.283.
- Castillo-Rogez, J. (2020). Future exploration of Ceres as an ocean world. *Nature Astronomy*, 4(8), 732-734.
- Clark, R. N., King, T. V., Klejwa, M., Swayze, G. A., Vergo, N. (1990). High spectral resolution reflectance spectroscopy of minerals. Journal of Geophysical Research: Solid Earth, 95(B8), 12653-12680.
- Cloutis, E. A., Hawthorne, F. C., Mertzman, S. A., Krenn, K., Craig, M. A., Marcino, D., Vilas, F. (2006). Detection and discrimination of sulphate minerals using reflectance spectroscopy. Icarus, 184(1), 121-157.
- Cloutis, E., Berg, B., Mann, P., Applin, D. (2016). Reflectance spectroscopy of low atomic weight and Na-rich minerals: Borates, hydroxides, nitrates, nitrites, and peroxides. Icarus, 264, 20-36.
- Comodi, P., Fastelli, M., Maturilli, A., Balic-Zunic, T., Zucchini, A. (2021). Emissivity and reflectance spectra at different temperatures of hydrated and anhydrous sulphates: A contribution to investigate the composition and dynamic of icy planetary bodies. Icarus, 355, 114132.

- Comodi, P., Nazzareni, S., Balić-Žunić, T., Zucchini, A., Hanfland, M. (2014). The high-pressure behavior of bloedite: A synchrotron single-crystal X-ray diffraction study. American Mineralogist, 99(2-3), 511-518.
- Comodi, P., Stagno, V., Zucchini, A., Fei, Y., Prakapenka, V. (2017). The compression behavior of blödite at low and high temperature up to∼ 10 GPa: Implications for the stability of hydrous sulfates on icy planetary bodies. Icarus, 285, 137-144.
- Cook, J. C., Dalle Ore, C. M., Protopapa, S., Binzel, R. P., Cartwright, R., Cruikshank, D. P.,Young, L. A. (2018). Composition of Pluto's small satellites: Analysis of New Horizons spectral images. Icarus, 315, 30-45.
- Cook, J. C., Desch, S. J., Roush, T. L., Trujillo, C. A., Geballe, T. R. (2007). Near-infrared spectroscopy of Charon: Possible evidence for cryovolcanism on Kuiper belt objects. The Astrophysical Journal, 663(2), 1406.
- Cruikshank, D. P., Umurhan, O. M., Beyer, R. A., Schmitt, B., Keane, J. T., Runyon, K. D., Ennico, K. (2019). Recent cryovolcanism in virgil fossae on Pluto. *Icarus*, *330*, 155-168.
- Dalle Ore, C. M., Cruikshank, D. P., Protopapa, S., Scipioni, F., McKinnon, W. B., Cook, J. C., Ennico, K. (2019). Detection of ammonia on Pluto's surface in a region of geologically recent tectonism. Science advances, 5(5), eaav5731.
- De Angelis, S., Carli, C., Tosi, F., Beck, P., Brissaud, O., Schmitt, B., Piccioni, G. (2019). NIR reflectance spectroscopy of hydrated and anhydrous sodium carbonates at different temperatures. Icarus, 317, 388-411.
- De Angelis, S., Tosi, F., Carli, C., Beck, P., Brissaud, O., Schmitt, B., Capaccioni, F. (2022). VIS-IR spectroscopy of magnesium chlorides at cryogenic temperatures. Icarus, 373, 114756.
- De Angelis, S., Tosi, F., Carli, C., Potin, S., Beck, P., Brissaud, O., Capaccioni, F. (2021). Temperature-dependent, VIS-NIR reflectance spectroscopy of sodium sulphatesulphates. Icarus, 357, 114165.
- De Sanctis, M. C., Ammannito, E., Raponi, A., Frigeri, A., Ferrari, M., Carrozzo, F. G., Russell, C. T. (2020). Fresh emplacement of hydrated sodium chloride on Ceres from ascending salty fluids. *Nature Astronomy*, *4*(8), 786-793.
- De Sanctis, M. C., Ammannito, E., Raponi, A., Marchi, S., McCord, T. B., McSween, H. Y. (2015). Ammoniated phyllosilicates with a likely outer Solar System origin on (1) Ceres. Nature, 528(7581), 241– 244.
- De Sanctis, M. C., Raponi, A., Ammannito, E., Ciarniello, M., Toplis, M. J., McSween, H. Y., Russell, C. T. (2016). Bright carbonate deposits as evidence of aqueous alteration on (1) Ceres. Nature, 536(7614), 54-57.
- Ehlmann, B. L., Hodyss, R., Bristow, T. F., Rossman, G. R., Ammannito, E., De Sanctis, M. C., Raymond, C. A. (2018). Ambient and cold-temperature infrared spectra and XRD patterns of ammoniated phyllosilicates and carbonaceous chondrite meteorites relevant to Ceres and other solar system bodies. Meteoritics & Planetary Science, 53(9), 1884-1901.
- Fastelli, M., Comodi, P., Maturilli, A., Zucchini, A. (2020). Reflectance Spectroscopy of Ammonium Salts: Implications for Planetary Surface Composition. Minerals, 10(10), 902.
- Fernandes, J. R., Ganguly, S., Rao, C. N. R. (1979). Infrared spectroscopic study of the phase transitions in CsNO3, RbNO3 and NH4NO3. Spectrochimica Acta Part A: Molecular Spectroscopy, 35(9), 1013-1020.
- Ferrari, M., De Angelis, S., De Sanctis, M. C., Ammannito, E., Stefani, S., Piccioni, G. (2019). Reflectance spectroscopy of ammonium-bearing phyllosilicates. Icarus, 321, 522-530.

- Fortes, A. D. (2000). Exobiological implications of a possible ammonia–water ocean inside Titan. *Icarus*, *146*(2), 444-452.
- Fortes, A. D., Choukroun, M. (2010). Phase behaviour of ices and hydrates. Space science reviews, 153(1-4), 185-218.
- Fortes, A. D., Grindrod, P. M., Trickett, S. K., Vočadlo, L. (2007). Ammonium sulphate on Titan: Possible origin and role in cryovolcanism. Icarus, 188(1), 139-153.
- Frost, R. L., Palmer, S. J. (2011). Infrared and infrared emission spectroscopy of nesquehonite $Mg(OH)(HCO_3)$ $2H_2O$ implications for the formula of nesquehonite. Spectrochimica Acta Part A: Molecular and Biomolecular Spectroscopy, 78(4), 1255-1260.
- Grundy, W. M., Binzel, R. P., Buratti, B. J., Cook, J. C., Cruikshank, D. P., Dalle Ore, C. M., Young, L. A. (2016). Surface compositions across Pluto and Charon. Science, 351(6279).
- Guidobaldi, G., Cambi, C., Cecconi, M., Comodi, P., Deneele, D., Paris, M., Zucchini, A. (2018). Chemo-mineralogical evolution and microstructural modifications of a lime treated pyroclastic soil. Engineering Geology, 245, 333-343.
- Hammond, N. P., Parmenteir, E. M., Barr, A. C. (2018). Compaction and Melt Transport in Ammonia-Rich Ice Shells: Implications for the Evolution of Triton. *Journal of Geophysical Research: Planets*, *123*(12), 3105-3118.
- Harlov, D.E., Andrut, M., Melzer, S., 2001a. Characterisation of NH4-phlogopite $(NH_4)(Mg_3)[AlSi_3O_{10}](OH)_2$ and ND_4-phlogopite $(ND_4)(Mg_3)[AlSi_3O_{10}](OD)_2$ using IR spectroscopy and Rietveld refinement of XRD spectra. Phys. Chem. Miner. 28,77–86.
- Harlov, D.E., Andrut, M., Pöter, B., 2001b. Characterization of buddingtonite $(NH_4)[AlSi_3O_8]$ and ND_4-buddingtonite $(ND_4)[AlSi_3O_8]$ using IR spectroscopy and Rietveld refinement of XRD spectra. Phys. Chem. Miner. 28, 188–198.
- Harlov, D.E., Andrut, M., Pöter, B., 2001c. Characterisation of tobelite $(NH_4)Al_2[AlSi_3O_{10}](OH)_2$ and ND_4-tobelite $(ND_4)Al_2[AlSi_3O_{10}](OH)_2$ using IR spectroscopy and Rietveld refinement of XRD data. Phys. Chem. Miner. 28, 268–276.
- Holloway, J. M., Dahlgren, R. A. (2002). Nitrogen in rock: occurrences and biogeochemical implications. Global biogeochemical cycles, 16(4), 65-1.
- Jia, X., Kivelson, M. G., Khurana, K. K., Kurth, W. S. (2018). Evidence of a plume on Europa from Galileo magnetic and plasma wave signatures. Nature Astronomy, 2(6), 459-464.
- Journaux, B., Kalousová, K., Sotin, C., Tobie, G., Vance, S., Saur, J., Brown, J. M. (2020). Large ocean worlds with high-pressure ices. Space Science Reviews, 216(1), 1-36.
- Kimura, J., Kamata, S. (2020). Stability of the subsurface ocean of Pluto. *Planetary and Space Science*, *181*, 104828.
- King, T.V.V., Clark, R.N., Calvin, W.M., Sherman, D.M., Brown, R.H. (1992). Evidence for ammonium-bearing minerals on Ceres. Science, 255, 1551–1553.
- Korchak, Y. M., Kapustyanyk, V. B., Partyka, M. V., & Rudyk, V. P. (2007). Temperature variation of the optical absorption edge for ammonium aluminum alum. Journal of Applied Spectroscopy, 74(2), 289-294.
- Krohn, M. D., & Altaner, S. P. (1987). Near-infrared detection of ammonium minerals. Geophysics, 52(7), 924-930.
- Larson, A.C.; Von Dreele, R.B. Generalized Structure Analysis System; University of California: San Diego, CA, USA, 1988.
- Levy, H. A., & Peterson, S. W. (1952). Neutron diffraction study of the crystal structure of ammonium chloride. Physical Review, 86(5), 766.

- Ligier, N., Poulet, F., Carter, J., Brunetto, R., Gourgeot, F. (2016). VLT/SINFONI observations of Europa: new insights into the surface composition. The Astronomical Journal, 151(6), 163.
- Loeffler, M. J., Raut, U., Baragiola, R. A. (2010). Radiation chemistry in ammonia-water ices. The Journal of chemical physics, 132(5), 054508.
- Max, J.-J., Chapados, C., 2013. Aqueous ammonia and ammonium chloride hydrates: Principal infrared spectra. J. Mol. Struct. 1046, 124–135.
- McCord, T. A., Hansen, G. B., Clark, R. N., Martin, P. D., Hibbitts, C. A., Fanale, F. P., Danielson, G. E. (1998). Non-water-ice constituents in the surface material of the icy Galilean satellites from the Galileo near-infrared mapping spectrometer investigation. Journal of Geophysical Research: Planets, 103(E4), 8603-8626.
- McCord, T. B., Hansen, G. B., Matson, D. L., Johnson, T. V., Crowley, J. K., Fanale, F. P., Ocampo, A. (1999). Hydrated salt minerals on Europa's surface from the Galileo near-infrared mapping spectrometer (NIMS) investigation. Journal of Geophysical Research: Planets, 104(E5), 11827-11851.
- Moriya, K., Matsuo, T., Suga, H., & Seki, S. (1977). On the phase transition of ammonium hexafluoroferrate (III). Bulletin of the Chemical Society of Japan, 50(8), 1920-1926.
- Mysen, B. (2019). Nitrogen in the Earth: abundance and transport. Progress in Earth and Planetary Science, 6(1), 1-15.
- Neveu, M.; Desch, S. J.; Castillo-Rogez, J. C (2017). Aqueous geochemistry in icy world interiors: Equilibrium fluid, rock, and gas compositions, and fate of antifreezes and radionuclides. Geochim. Cosmochim. Acta, 2017,212, 324-371.
- Nuth III, J. A., Abreu, N., Ferguson, F. T., Glavin, D. P., Hergenrother, C., Hill, H. G., & Walsh, K. (2020). Volatile-rich Asteroids in the Inner Solar System. The Planetary Science Journal, 1(3), 82.
- Pilorget, C., Okada, T., Hamm, V., Brunetto, R., Yada, T., Loizeau, D., Bibring, J. P. (2021). First compositional analysis of Ryugu samples by the MicrOmega hyperspectral microscope. Nature Astronomy, 1-5.
- Poch, O., Istiqomah, I., Quirico, E., Beck, P., Schmitt, B., Theulé, P., Tosi, F. (2020). Ammonium salts are a reservoir of nitrogen on a cometary nucleus and possibly on some asteroids. Science, 367(6483).
- Pommerol, A., Schmitt, B., Beck, P., & Brissaud, O. (2009). Water sorption on martian regolith analogs: Thermodynamics and near-infrared reflectance spectroscopy. Icarus, 204(1), 114-136.
- Quinn, R. C., Chittenden, J. D., Kounaves, S. P., & Hecht, M. H. (2011). The oxidation-reduction potential of aqueous soil solutions at the Mars Phoenix landing site. Geophysical research letters, 38(14).
- Rauscher, B. J., Fox, O., Ferruit, P., Hill, R. J., Waczynski, A., Wen, Y., Strada, P. (2007). Detectors for the James Webb Space Telescope Near-Infrared Spectrograph. I. Readout Mode, Noise Model, and Calibration Considerations. Publications of the Astronomical Society of the Pacific, 119(857), 768.
- Rietveld, H.M. (1969). A profile refinement method for nuclear and magnetic structures. Journal of Applied Crystallography, 2, 65–71
- Ross, S.D., (1974). Sulphates and other oxy-anions of group VI. In: Farmer, V.C. (Ed.), The Infrared Spectra of Minerals. Mineralogical society, London, pp. 423–444.

- Russell, C. T., & Raymond, C. A. (2011). The dawn mission to Vesta and Ceres. Space Sci. Rev, 163, 3-23.
- Salisbury, J. W., & Walter, L. S. (1989). Thermal infrared (2.5–13.5 μm) spectroscopic remote sensing of igneous rock types on particulate planetary surfaces. Journal of Geophysical Research: Solid Earth, 94(B7), 9192-9202.
- Schlemper, E. O., Hamilton, W. C. (1966). Neutron-Diffraction Study of the Structures of Ferroelectric and Paraelectric Ammonium Sulphate. The Journal of Chemical Physics, 44(12), 4498-4509.
- Schmitt, B., Philippe, S., Grundy, W. M., Reuter, D. C., Côte, R., Quirico, E., Weaver, H. A. (2017). Physical state and distribution of materials at the surface of Pluto from New Horizons LEISA imaging spectrometer. *Icarus*, *287*, 229-260.
- Schumaker, N. E., Garland, C. W. (1970). Infrared investigation of structural and ordering changes in ammonium chloride and bromide. The Journal of Chemical Physics, 53(1), 392-407.
- Sefton-Nash, E., Catling, D. C., Wood, S. E., Grindrod, P. M., Teanby, N. A. (2012). Topographic, spectral and thermal inertia analysis of interior layered deposits in Iani Chaos, Mars. Icarus, 221(1), 20-42.
- Sekine, A., Sumita, M., Osaka, T., Makita, Y. (1988). Ferroelectricity and dielectric relaxation in $NH_4Al(SO_4)_2{\cdot}12H_2O$. Journal of the Physical Society of Japan, 57(11), 4004-4010.
- Sergeeva, A. V., Zhitova, E. S., Bocharov, V. N. (2019). Infrared and Raman spectroscopy of tschermigite, $(NH_4)Al(SO_4)_2\ 12H_2O$. Vibrational Spectroscopy, 105, 102983.
- Simon, P. (1989). Phonon spectra of $NH_4H_2PO_4$ in the para-and antiferroelectric phases obtained by infrared reflectivity. Journal de Physique, 50(24), 3477-3487.
- Smith, D. (1994). Hindered rotation of the ammonium ion in the solid state. Chemical reviews, 94(6), 1567-1584.
- Sparks, W. B., Hand, K. P., McGrath, M. A., Bergeron, E., Cracraft, M., Deustua, S. E. (2016). Probing for evidence of plumes on Europa with HST/STIS. The Astrophysical Journal, 829(2), 121.
- Stefov, V., Šoptrajanov, B., Spirovski, F., Kuzmanovski, I., Lutz, H. D., Engelen, B. (2004). Infrared and Raman spectra of magnesium ammonium phosphate hexahydrate (struvite) and its isomorphous analogues. I. Spectra of protiated and partially deuterated magnesium potassium phosphate hexahydrate. *Journal of Molecular Structure*, *689*(1-2), 1-10.
- Stern, S. A., Weaver, H. A., Steffl, A. J., Mutchler, M. J., Merline, W. J., Buie, M. W., Spencer, J. R. (2006). A giant impact origin for Pluto's small moons and satellite multiplicity in the Kuiper belt. Nature, 439(7079), 946-948.
- Tenzer, L., Frazer, B. C., Pepinsky, R. (1958). A neutron structure analysis of tetragonal $NH_4(H_2PO_4)$. Acta Crystallographica, 11(7), 505-509.
- Theoret, A., & Sandorfy, C. (1964). Infrared spectra and crystalline phase transitions of ammonium nitrate. Canadian Journal of chemistry, 42(1), 57-62.
- Toby, B. H. (2001). EXPGUI, a graphical user interface for GSAS. Journal of applied crystallography, 34(2), 210-213.
- Vainshtein, B.K (1956). Refinement of the structure of the group NH_4 in the structure of ammonium chloride. Dokl. Akad. Nauk SSSR, 12, 18–24.
- Waddington, T. C. (1958). 881. Infrared spectra, structure, and hydrogen-bonding in ammonium salts. Journal of the Chemical Society (Resumed), 4340-4344.

- West, C. D. (1932). The crystal structure of rhombic ammonium nitrate. Journal of the American Chemical Society, 54(6), 2256-2260.
- Wu, H. B., Chan, M. N., Chan, C. K. (2007). FTIR characterization of polymorphic transformation of ammonium nitrate. Aerosol Science and Technology, 41(6), 581-588.
- Zhu, Y., Li, Y., Ding, H., Lu, A., Li, Y., Wang, C. (2020). Infrared emission properties of a kind of natural carbonate: Interpretation from mineralogical analysis. Physics and Chemistry of Minerals, 47(3), 1-15.